

Simulation of GaN CAVETs in Silvaco Atlas

by

Andrew Warren

A Thesis Presented in Partial Fulfillment  
of the Requirements for the Degree  
Master of Science

Approved April, 2019 by the  
Graduate Supervisory Committee

Dragica Vasileska, Chair  
Steven Goodnick  
Yuji Zhao

ARIZONA STATE UNIVERSITY

May 2019

## ABSTRACT

Gallium Nitride (GaN) based Current Aperture Vertical Electron Transistors (CAVETs) present many appealing qualities for applications in high power, high frequency devices. The wide bandgap, high carrier velocity of GaN make it ideal for withstanding high electric fields and supporting large currents. The vertical topology of the CAVET allows for more efficient die area utilization, breakdown scaling with the height of the device, and burying high electric fields in the bulk where they will not charge interface states that can lead to current collapse at higher frequency.

Though GaN CAVETs are promising new devices, they are expensive to develop due to new or exotic materials and processing steps. As a result, the accurate simulation of GaN CAVETs has become critical to the development of new devices. Using Silvaco Atlas 5.24.1.R, best practices were developed for GaN CAVET simulation by recreating the structure and results of the pGaN insulated gate CAVET presented in chapter 3 of [8].

From the results it was concluded that the best simulation setup for transfer characteristics, output characteristics, and breakdown included the following. For methods, the use of Gummel, Block, Newton, and Trap. For models, SRH, Fermi, Auger, and impact self. For mobility, the use of GANSAT and manually specified saturation velocity and mobility (based on doping concentration). Additionally, parametric sweeps showed that, of those tested, critical CAVET parameters included channel mobility (and thus doping), channel thickness, Current Blocking Layer (CBL) doping, gate overlap, and aperture width in rectangular devices or diameter in cylindrical devices.

## TABLE OF CONTENTS

	Page
LIST OF TABLES .....	iii
LIST OF FIGURES .....	iv
CHAPTER	
INTRODUCTION .....	1
1.1 Background .....	2
1.2 Advantages and Applications of GaN.....	2
1.3 CAVET and HEMT Devices .....	7
Experimental Device and Results .....	11
2.1 Experimental Device Structure and Fabrication .....	12
2.2 Experimental Results .....	15
Simulated Device and Results .....	19
3.1 Initial GaN Experiment.....	20
3.2 Device Simulation Setup.....	24
3.3 Parametric Sweeps .....	27
3.4 Final Setup and Results.....	35
Conclusion and Future Work .....	42
4.1 Conclusion .....	43
4.2 Future Work .....	43
REFERENCES .....	46
APPENDIX	
A. TRANSFER CHARACTERISTIC SIMULATION INPUT DECK .....	48

## LIST OF TABLES

Table	Page
Table 1-1: Semiconductor Material Properties .....	6
Table 2-1: Device Vertical Dimensions and Doping .....	14
Table 2-2: Device Horizontal Dimensions .....	14
Table 2-3: Box Profile Implant .....	17
Table 3-1: Mobility from Doping .....	26
Table 3-2: Corrected Values .....	36

## LIST OF FIGURES

Figure	Page
Figure 1-1: Wurtzite GaN Band Diagram.....	3
Figure 1-2: Si Band Structure .....	4
Figure 1-3: (a) The Structure of a Green GaN LED [11]. (b) The Visible Spectrum.....	5
Figure 1-4: (a) Structure of a HEMT Showing a Lateral Breakdown Relation (b) Structure of a CAVET with a Vertical Breakdown Relation.....	8
Figure 2-1: Structure of the pGaN Insulated Gate CAVET.....	12
Figure 2-2: pGaN Insulated Gate CAVET Fabrication Process Flow .....	13
Figure 2-3: (a) The Experimental Output Characteristics (b) The Experimental Transfer Characteristics.....	15
Figure 2-4: Experimental Breakdown Characteristics .....	16
Figure 2-5: (a) Box Implant Output Characteristics (b) Box Implant Transfer Characteristics.....	17
Figure 2-6: Box Implant Breakdown Characteristics .....	18
Figure 3-1: Monte Carlo Simulation of GaN Electron Velocity vs Electric Field .....	20
Figure 3-2: GaN Electron Velocity vs Field for $N_d=1E17$ at 77K (Dotted), 150K (Solid), 300K (Dashed), 500K (Circles), and 1000K (Pluses).....	21
Figure 3-3: Simulated Results for Mobility Values of 200 to 1600 $\text{cm}^2/\text{V}/\text{sec}$ .....	23
Figure 3-4: Simulated Device Mesh Around the Channel and Aperture.....	25
Figure 3-5: Simulated Device Cross Section.....	25
Figure 3-6: (a) GaN Hole Mobility vs Concentration (b) GaN Electron Mobility vs Concentration for Various Compensation Values .....	26

Figure	Page
Figure 3-7: CBL Doping Sweep .....	27
Figure 3-8: Conduction and Valence Band Energy Through the Gate, pGaN Insulator and into the Channel .....	28
Figure 3-9: Extended CBL Doping Sweep .....	29
Figure 3-10: Gate Insulator Doping Sweep .....	30
Figure 3-11: Channel Mobility Sweep.....	31
Figure 3-12: Aperture Mobility Sweep.....	31
Figure 3-13: Drift Region Mobility Sweep.....	32
Figure 3-14: Drain Region Mobility Sweep .....	32
Figure 3-15: Gate Overlap Sweep.....	33
Figure 3-16: Aperture Length Sweep .....	34
Figure 3-17: Drain Resistance Sweep.....	34
Figure 3-18: Channel Thickness Sweep .....	35
Figure 3-19: Simulated ID-VG Curve and Experimental Data .....	37
Figure 3-20: Simulated and Experimental ID-VD Curves .....	37
Figure 3-21: Breakdown of the Simulated pGaN Insulated Gate CAVET.....	38
Figure 3-22: Log Scale Electron Concentration at Breakdown .....	39
Figure 3-23: Electric Field Magnitude at Breakdown .....	39
Figure 3-24: Log Scale Impact Ionization Rate.....	40
Figure 3-25: Simulated Device Log Scale Electron Concentration at 70V Drain Bias....	40
Figure 3-26: Simulated Device Electric Field Profile at 70V Drain Bias.....	41

## Chapter 1

### INTRODUCTION

## 1.1 Background

The foundation for the work in this thesis is based on the PhD dissertation of Saptarshi Mandal. In [8], Mandal covers the fabrication and testing of physical Gallium Nitride (GaN) Current Aperture Vertical Electron Transistor (CAVET) devices for Radio Frequency (RF) amplifier applications. GaN is a wide bandgap semiconductor that has become an intriguing option for high power electronics due to its higher breakdown voltage, larger electron saturation velocity, and comparable thermal conductivity when compared to Silicon (Si) [1]. These advantages however, come with the caveat of significantly higher manufacturing costs due to the nature of a new technology and the use of expensive substrates like Sapphire. This high cost makes accurate TCAD design and simulation all the more important for experimenting with designs in simulation before going to physical prototypes and production devices. The primary goal of this thesis is therefore to cover the necessary considerations and settings for accurate simulation of GaN in Silvaco Atlas 5.24.1.R. To do this, the p-GaN insulated gate CAVET discussed in sections 3.1 to 3.3 of [8] will serve as the physical device and experimental data to model and reproduce. In addition to the primary objective, the development of the input deck and experiments that lead to the final conclusion will be covered, as well as exploring the effects several device parameters have on performance.

## 1.2 Advantages and Applications of GaN

GaN is a direct bandgap III-V Nitride semiconductor with a wide bandgap (3.4eV), leading to several advantages over traditional semiconductors like Si [16]. GaN may have



a zincblende or wurtzite crystalline structure, though the wurtzite is much more common and will be assumed throughout this paper.

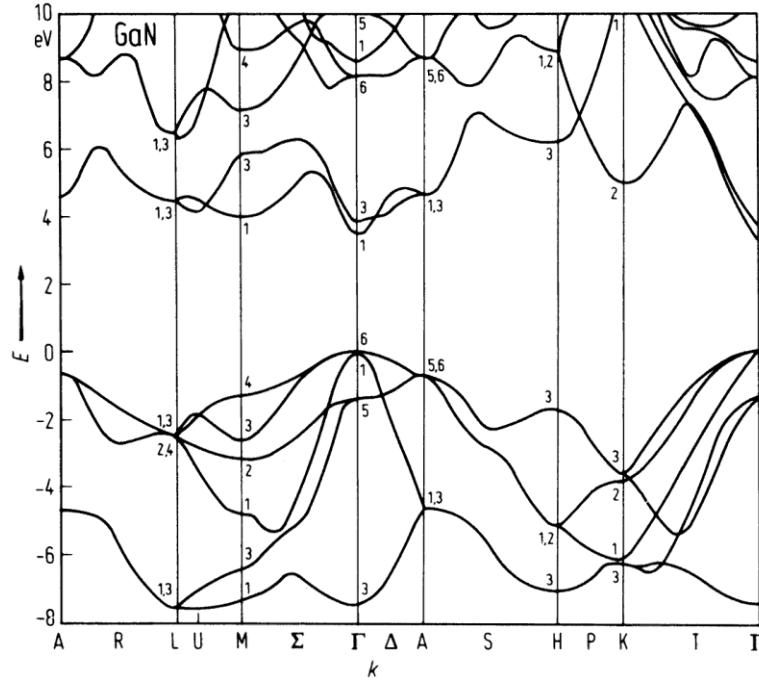


**Figure 1-1: Wurtzite GaN Band Diagram [5]**

As stated in the previous section, manufacturing GaN devices is relatively expensive and as such, it is best to use GaN in an application where its properties are the most beneficial. Being a direct bandgap semiconductor, one of these applications is in optical devices. For both photon absorption and emission, direct bandgap semiconductors can offer significant efficiency improvements over indirect bandgap semiconductors like Si by allowing direct photon emission and absorption without requiring phonons for lateral movement in K-space. Figure 1-2 shows the band diagram of Si with a misaligned Conduction Band Minimum (CBM) and Valence Band Maximum (VBM), while figure 1-1 shows the band diagram of GaN with aligned CBM and VBM. GaN has been used in advanced solar cell designs, often in the form of InGaN where the amount of Indium can

be used to adjust the bandgap from 0.7-3.4eV. This flexibility allows InGaN based panels with multiple junctions to cover almost all of the usable solar emission range, which spans from about 0.5-3eV [9].

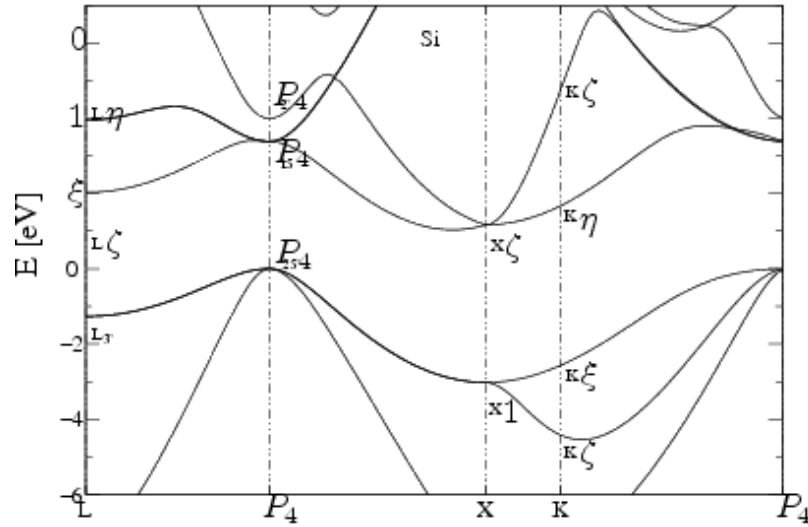


**Figure 1-2: Si Band Structure [19]**

Many of the properties that make GaN an excellent choice for photon absorption in photovoltaics also make it ideal for photon emission in Light Emitting Diodes (LEDs). GaN based LEDs began development in the 1970s when GaN growth was still in its early stages, resulting in the first GaN based LEDs being constructed in a Metal Insulator Semiconductor (MIS) structure since p-type GaN had yet to be developed [11]. Further development of both GaN processing and LED technology eventually led to the first p-n junction GaN LED in 1989 and the introduction of high brightness blue LEDs in 1993. Similar to photovoltaics, the use of InGaN allowed for bandgap engineering by adjusting the Indium-Nitride mole fraction, enabling the construction of high brightness blue, violet, and green LEDs [11]. Figure 1-3 a. shows the structure of a green single quantum well (SQW) LED grown on a sapphire substrate. Figure 1-3 b. shows the visible spectrum

in frequency, wavelength, and energy, illustrating how engineering the bandgap will produce different colors.

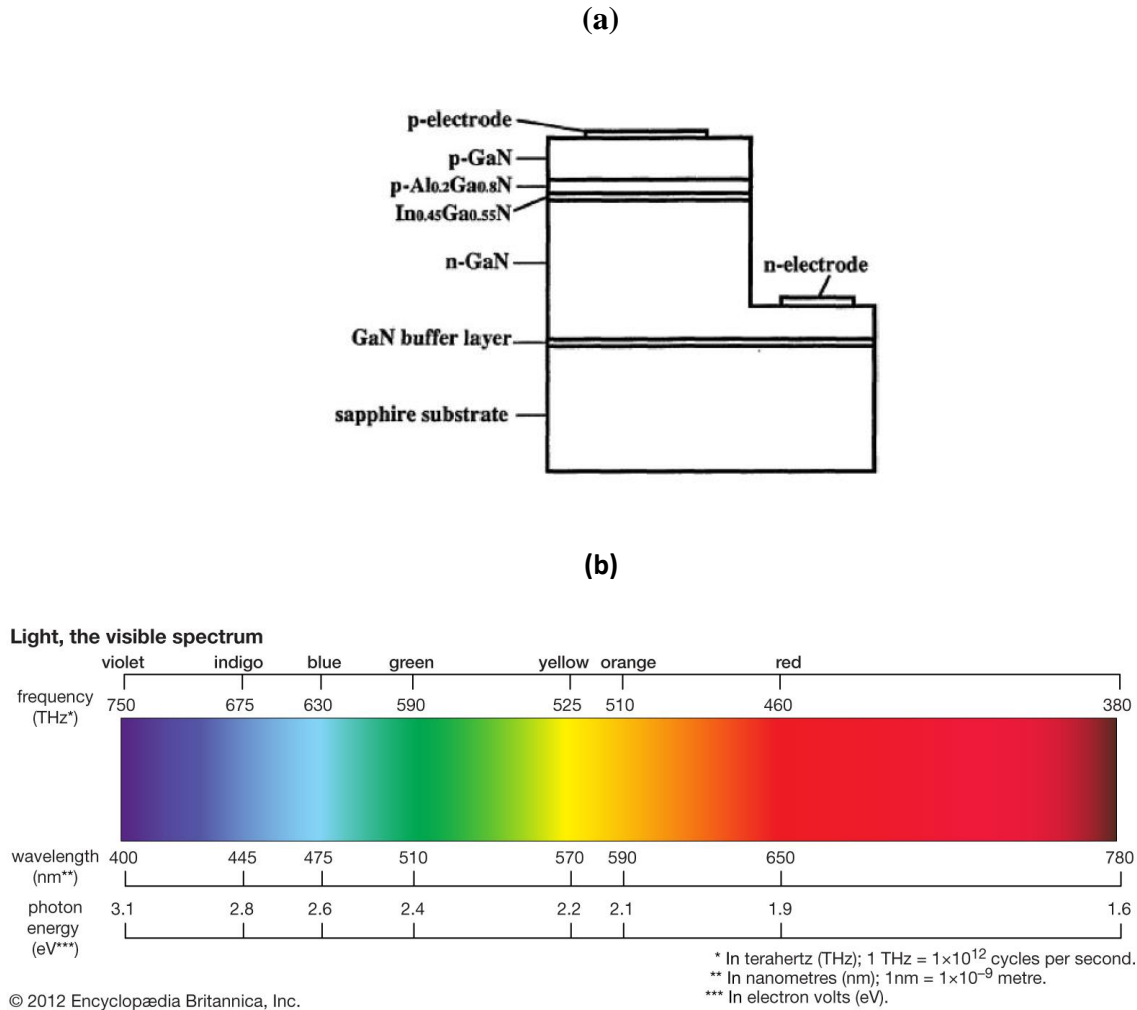


**Figure 1-3: (a) The Structure of a Green GaN LED [11]. (b) The Visible Spectrum [15].**

Beyond optoelectronics, GaN also has applications in power electronics due to its high temperature and high frequency operation capabilities. Aside from GaN, Silicon Carbide (SiC) and Gallium Arsenide (GaAs) are two other competing materials for use in high power electronics. Table 1-1 compares several parameters of various semiconductors relevant to power devices.

**Table 1-1: Semiconductor Material Properties [18]**

Material	$E_g$ (eV)	$\epsilon_r$	$\kappa$ (W °K cm <sup>-1</sup> )	$E_c$ (V cm <sup>-1</sup> )
Si	1.12	11.9	1.5	3.00E+05
GaAs	1.43	12.5	0.54	4.00E+05
InP	1.34	12.4	0.67	4.50E+05
3C-SiC	2.3	9.7	4	1.80E+06
4H-SiC	3.2	10	4	3.50E+06
6H-SiC	2.86	10	4	3.80E+06
GaN	3.4	9.5	1.3	3.30E+06
Diamond	5.6	5.5	20-30	5.00E+06

From this data, it can be seen that both GaN and SiC have an advantage over GaAs and Si in terms of bandgap and critical electric field, allowing them to have much higher breakdown voltage and thus much higher blocking capability. This property is particularly important in high power devices as the breakdown field is a critical component of how much power a device can handle. In addition to high breakdown, the ideal material for high power electronics should be able to operate at high temperatures and have a high thermal conductivity to dissipate heat. Both GaN and SiC meet the first of these two criteria with high melting points of 2500C and 2830C respectively [7]. The thermal conductivity of GaN is higher than GaAs, but comparable to that of Si. SiC on the other hand, has a notably higher thermal conductivity than all three, though wurtzite GaN can take advantage of this as it may be grown on a hexagonal SiC substrate with a lattice mismatch on the order of 3% [18]. Lastly, modern high power electronics often involve high current and high frequency operation, such as in RF amplifiers. This lends another advantage to wide bandgap semiconductors since they often have high saturation velocities which allow large currents. Both SiC and GaN based devices are capable of operating at X-band (8-12GHz) frequencies, however GaN devices that implement

AlGa<sub>N</sub>/Ga<sub>N</sub> heterojunctions have the advantage of developing a Two Dimensional Electron Gas (2DEG) under the junction due to polarization charge. This 2DEG allows for low resistivity, low noise, and higher frequencies than SiC based devices.

### 1.3 CAVET and HEMT Devices

CAVETs are a vertical transistor topology that offers high breakdown voltage, high frequency operation, and efficient die area utilization. High Electron Mobility Transistors (HEMTs) are planar devices that are often made of the same materials and feature similar gate and channel construction. HEMTs have been commercially available since the early 1980s and have primarily found applications in RF devices such as microwave satellite communications and radio telescopes due to their stable high frequency operation [10]. The potential higher frequency and power capabilities of the CAVET indicate that the device may be a replacement for HEMTs in many of these applications looking to extend the capabilities of such RF equipment.

HEMTs operate on a similar basic principal to a standard MOSFET (Metal Oxide Semiconductor Field Effect Transistor). It is a planar device with source and drain contacts to either side of a gate that modulates the channel beneath it. The gate may either be insulated by a material such as a dielectric, or it may be a Schottky gate. A typical Ga<sub>N</sub> HEMT is a depletion mode device where a high mobility 2DEG channel is normally formed at the AlGa<sub>N</sub>/Ga<sub>N</sub> barrier when no gate bias is present. A gate bias would then be used to modulate the channel by depleting it of carriers.

Similar to the HEMT, the typical Ga<sub>N</sub> CAVET is a depletion mode device and has an insulated or Schottky gate. Beneath the gate there may be either a AlGa<sub>N</sub>/Ga<sub>N</sub> junction

forming a 2DEG or simply a conducting nGaN layer. The channel is again modulated by applying a bias to the gate to deplete the channel. Unlike a HEMT however, the current path is vertical between the source and drain. Below the source is a Current Blocking Layer (CBL) that prevents current flow directly between the source and drain, forcing it to flow through an aperture. The aperture is shown in figure 1-4 (b), the region between the two CBLs, the channel, and drift region. With the application of a gate bias, the CBL allows the gate to pinch off the channel by expanding the depletion region below it, essentially “corking” the aperture shut.

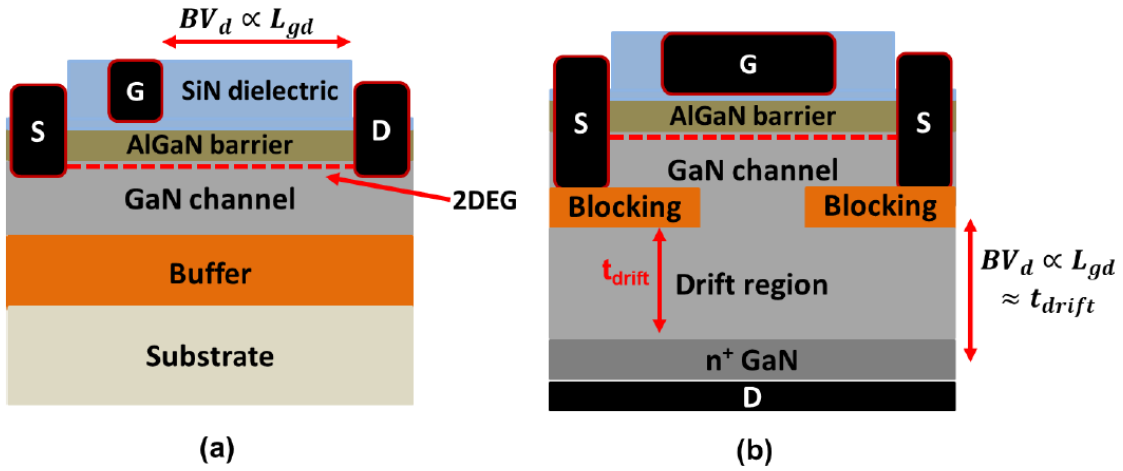


**Figure 1-4: (a) Structure of a HEMT Showing a Lateral Breakdown Relation. (b) Structure of a CAVET with a Vertical Breakdown Relation [8].**

Shown in figure 1-4 is the basic structure of a GaN HEMT and CAVET with a dielectric gate insulator and an AlGaIn/GaN heterojunction to create a 2DEG in the channel. Also illustrated in figure 1-4 is how the breakdown voltage scales; increasing with increasing lateral gate to drain distance in a HEMT and vertically with gate to drain distance in a CAVET. This relation leads to the first advantage of the CAVET over the HEMT where high breakdown voltages are required. In order to increase the breakdown

of a device, the electric field must be spread over a longer distance to avoid reaching the critical electric field of the material, particularly near the edge of the gate closest to the drain where the highest fields occur [3]. In a HEMT this means extending the gate to drain distance laterally and using more die area. Die area on any electronics grade substrate is very expensive and in the case of GaN devices, this is especially true as they are constructed on less common and sometimes exotic substrates like sapphire. The advantage of the CAVET in this regard is that the gate to drain distance is vertical, so extending this distance for higher breakdown would entail growing a taller drift region. Depending on the growth process, this may take longer to construct than a comparable HEMT, but with the benefit of saving valuable die area.

In addition to facilitating device breakdown due to high localized electric fields, the high electric fields near the surface between the gate and drain in a HEMT lead to DC-RF dispersion. This occurs when the high electric field charges surface states which, under high frequency operation, will not transition as fast as the gate [3]. This leaves charged states that will modulate the channel independent of the gate until they are discharged, degrading high frequency performance. The CAVET is able to resolve this issue by keeping the high electric field in the bulk material, away from the surface states [3]. It has been shown in [3] that for a CAVET with a gate that fully covers the aperture, the DC-RF dispersion is negligible. In the same paper it was also demonstrated that offsetting the gate from the aperture and drain exposes the current path to a high field region near the gate edge, resulting in the same interface state charging seen in HEMTs. From the discussion in this section, it can be concluded that CAVETs offer several benefits over

traditional HEMTs, though an understanding of the mechanisms that degrade performance is crucial for developing optimized designs.



## Chapter 2

### Experimental Device and Results

## 2.1 Experimental Device Structure and Fabrication

The physical device providing the experimental results that will serve as a baseline for the simulated device is the pGaN insulated gate CAVET discussed in Ch 3.1-3.3 of [8]. This device was chosen for simulation since the construction and simulation of the device was well documented by Mandal, offering the best chance for accurate re-creation. The following will discuss the structure of the device and its fabrication.

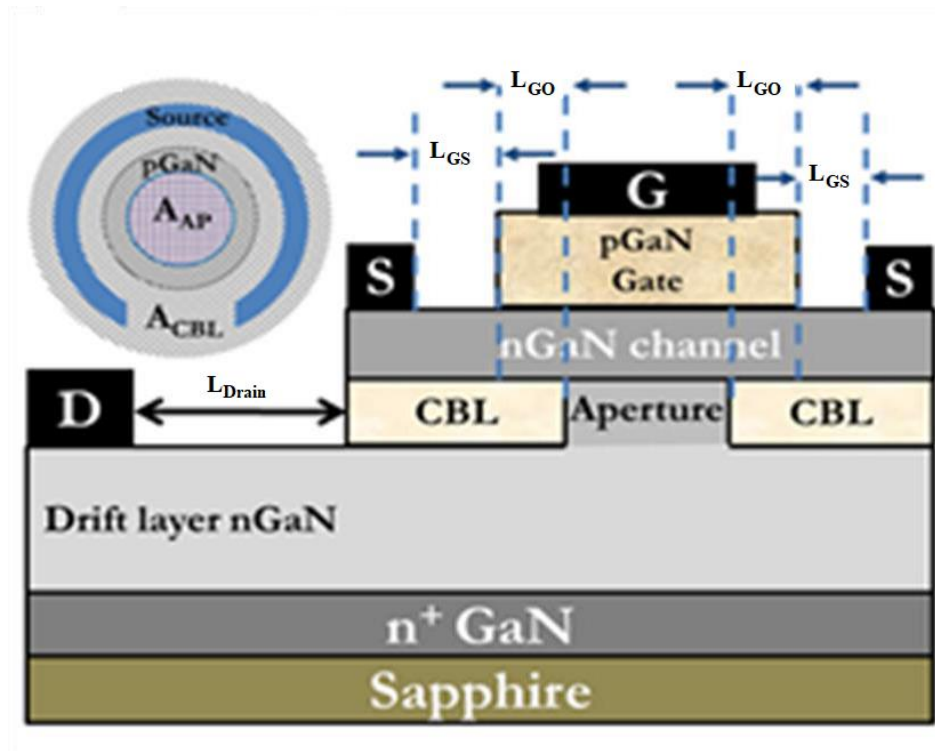


**Figure 2-1: Structure of the pGaN Insulated Gate CAVET [8].**

Figure 2-1 shows a cross-sectional and top down view of the CAVET. The experimental device is circular, which differs from the rectangular simulated device. The possible effects of this difference will be discussed further in the simulation chapter. Also to be noted from this diagram is that the drain is offset from the aperture and on top of the drift layer. This is a consequence of the non-conducting sapphire substrate removing the

possibility of using a back contact for the drain. The sapphire substrate was a compromise in order to achieve better control over the drift layer doping, particularly for low doping concentrations [8].

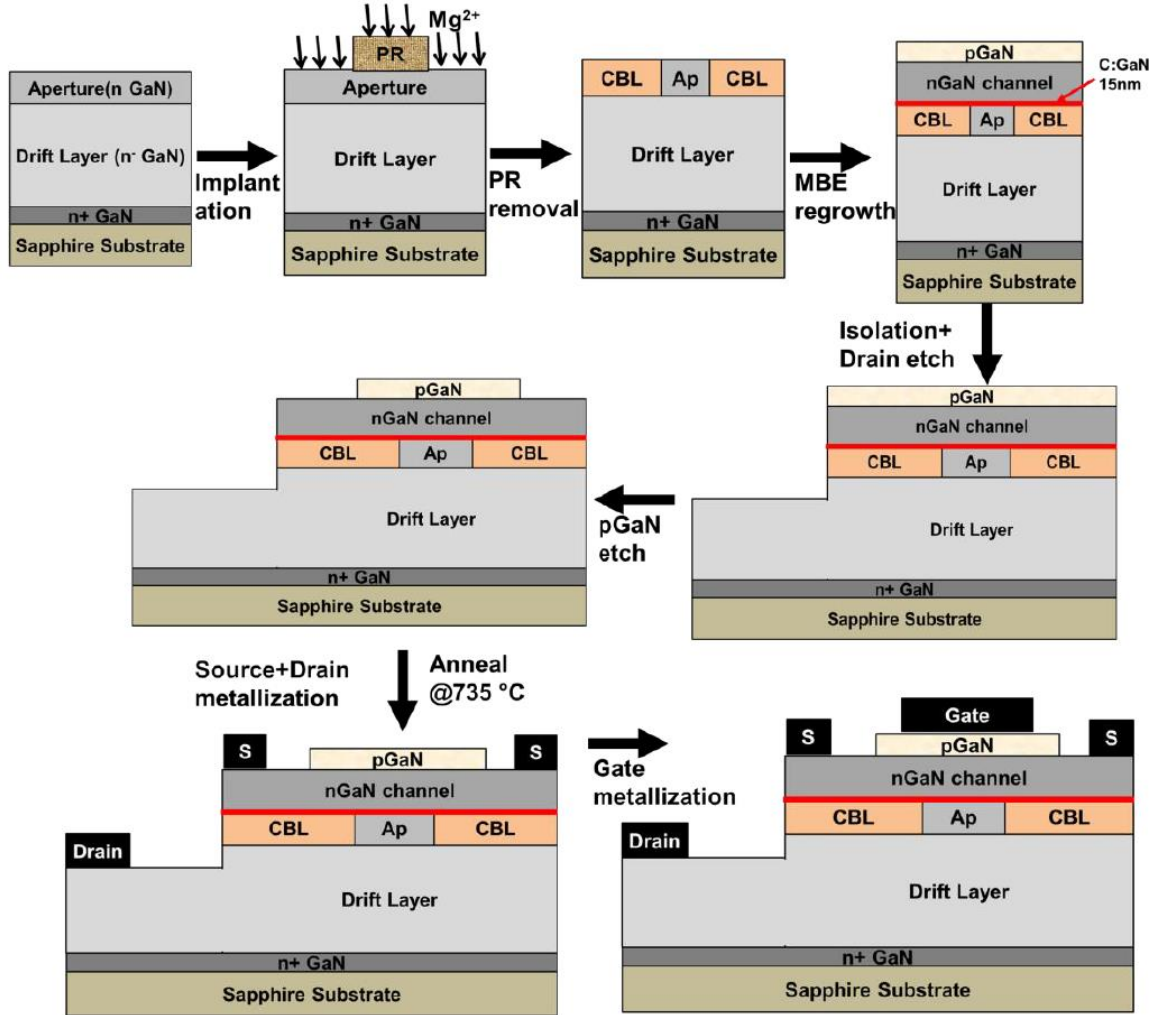


**Figure 2-2: pGaN Insulated Gate CAVET Fabrication Process Flow [8].**

Figure 2-2 shows the process flow used to fabricate the CAVET. The carbon doped layer, shown as the red layer, was implemented to prevent the absorption of Si atoms during processing which can lead to parasitic channel formation [8]. The vertical

dimensions and doping levels are given in table 2-1 while the lateral dimensions are given in table 2-2.

**Table 2-1: Device Vertical Dimensions and Doping**

Layer	Thickness ( $\mu\text{m}$ )	Doping Type	Concentration ( $\text{cm}^{-3}$ )	Notes
Sapphire substrate	450	N/A	N/A	
n+ drain region	1	n-type (Si)	$2.00\text{E}+18$	
n- drift layer	6	n-type (Si)	$5.00\text{E}+15$	
Aperture layer	0.3	n-type (Si)	$2.00\text{E}+16$	
CBL	0.3	p-type (Mg)	80keV $\text{Mg}^{2+}$ ion implantation with a dose of $1\text{E}15 \text{ cm}^{-2}$	Implanted into the aperture layer, patterned with photoresist.
Carbon doped layer	0.015	C	$6.00\text{E}+18$	
Channel layer	0.3	n-type (Si)	$3.00\text{E}+17$	
Gate insulator	0.1	p-type (Mg)	$5.00\text{E}+19$	

**Table 2-2: Device Horizontal Dimensions**

Dimension	Length ( $\mu\text{m}$ )
Aperture Length	5
Gate Overlap	4
Gate to Source	4

The pGaN gate insulator in this design takes advantage of the high breakdown of a GaN p-n junction to achieve a device breakdown above 400V. In Ch 2 of [8], a similar CAVET is tested with an  $\text{Al}_2\text{O}_3$  dielectric gate insulator. Tests of the CBL and gate insulator showed that the dielectric was the limiting factor in the device's breakdown performance. With the top contact of the test structure held at 0V, the CBL was able to withstand a drain bias of 400V without breaking down. The dielectric however, with the gate held at the pinch-off of -25V, was only able to handle a drain bias of about 30V [8].

## 2.2 Experimental Results

The experimental results outlined in this section will be the baseline to replicate as closely as possible with the simulated device. All the current values given in these results are in  $\text{A}/\text{cm}^2$ , where the area enclosed by the source contacts is the area the total current is divided by to achieve a current density.

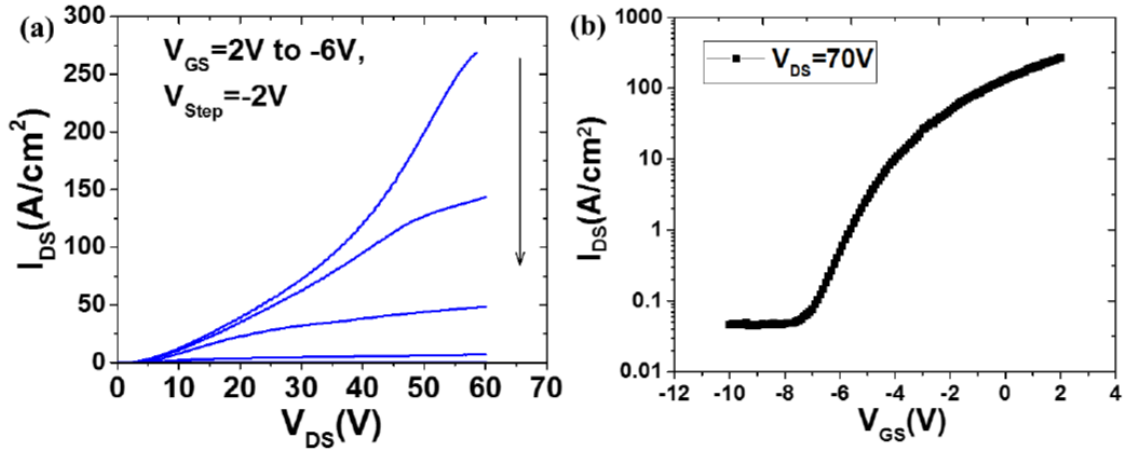


**Figure 2-3: (a) The Experimental Output Characteristics. (b) The Experimental Transfer Characteristics [8].**

Figure 2-3 (b) show the experimental transfer characteristics with a drain bias of 70V and a gate sweep from 2 to -10V. Pinch-off of the channel occurs around -9V and the peak current is just under 500  $\text{A}/\text{cm}^2$ . Figure 2-3 (a) shows the output characteristics of the device with gate biases from 2 to -6V in 2V decrements. For each gate bias, the drain is swept from 0 to 60V. It should be noted that these output curves seem to indicate that the device is very resistive, particularly on the two highest gate biases as they slowly curve upward through a majority of the sweep and only appear to be reaching saturation above 50V. An optimal device would be expected to rise quickly to saturation and remain at a relatively stable current for the remainder of the sweep.

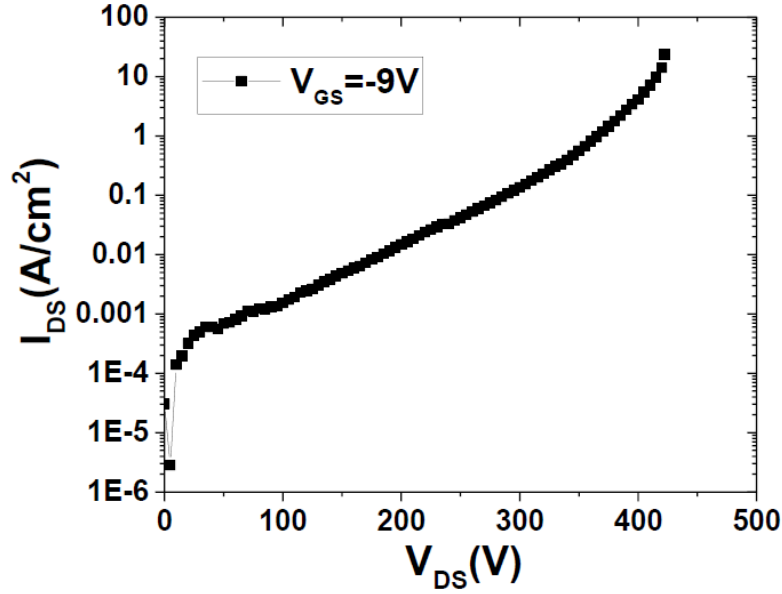


**Figure 2-4: Experimental Breakdown Characteristics [8].**

Figure 2-4 shows the breakdown characteristics of the experimental device. The test was performed by holding the gate held below pinch-off and sweeping the drain bias, resulting in a breakdown of 422V. Since breakdown was expected to occur from either a failure of the gate p-n junction or the CBL, Mandal performed two further breakdown experiments on an n-CBL-n structure with no aperture and a p-n junction gate insulator. The two structures broke down at 450 and 560V respectively. This lead to the conclusion that the CBL was now the limiting factor in device breakdown performance. In order to improve upon this, a new device was fabricated with a box profile implanted CBL. This CBL utilizes several implant steps with varying energy and dose to achieve a more uniform profile than the single 80 keV implant used in the previous device. Table 2-3 shows the energy and dose used for the box implant.

**Table 2-3: Box Profile Implant**

Implant Species	Energy (keV)	Dose (cm <sup>-2</sup> )
Mg <sup>2+</sup>	300	2.50E+14
Mg <sup>2+</sup>	225	2.50E+14
Mg <sup>2+</sup>	110	1.30E+14
Mg <sup>2+</sup>	55	6.00E+13
Mg <sup>2+</sup>	25	1.00E+13
Mg <sup>2+</sup>	10	1.00E+13

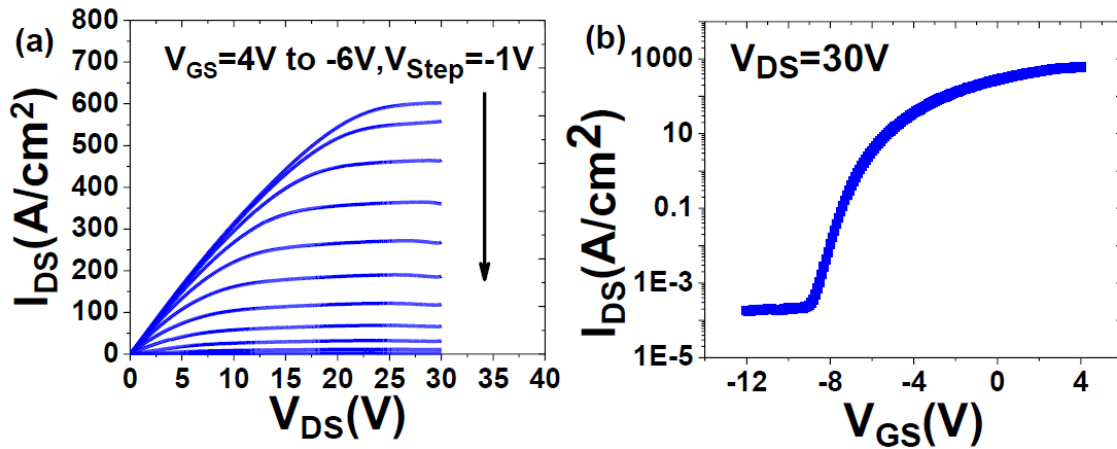
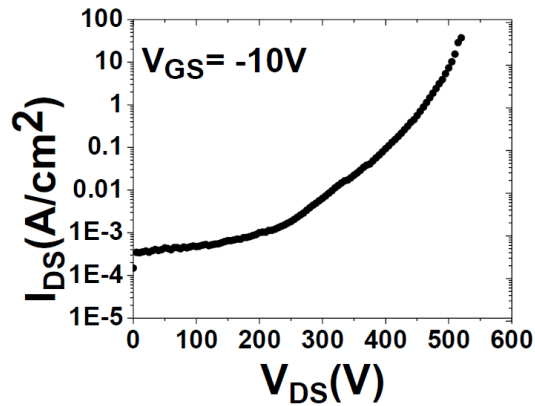
**Figure 2-5: (a) Box Implant Output Characteristics. (b) Box Implant Transfer Characteristics [8].**

Figure 2-6 (a) shows the output characteristics of the experimental CAVET with the box profile CBL implant. A drain sweep of 0-30V and gate biases of 4 to -6 were used in 1V decrements. While this device does seem to exhibit some resistance, it is much better than the single implant device. Figure 2-6 (b) shows the transfer characteristics for the device with a drain bias of 30V and a gate sweep from 4 to -12V. Compared to the single implant CBL, this device had a more negative pinch-off at -10V and passed more current at any given bias.

The breakdown characteristics for the box profile CBL are shown in figure 2-6. With the gate biased below pinch-off, this device reached breakdown at 520V. Following the test, Mandal again performed individual breakdown tests on the CBL and p-n junction gate insulator to determine the limiting factor. The CBL reached breakdown around 520V while the p-n junction was able to block over 600V.



**Figure 2-6: Box Implant Breakdown Characteristics [8].**



## Chapter 3

### Simulated Device and Results

### 3.1 Initial GaN Experiment

The goal of this project is to simulate GaN devices as accurately as possible, therefore the first step taken towards this end was to ensure the properties of GaN itself could be simulated. To start, a simulation of electron velocity vs electric field was performed to establish what models and methods are necessary to properly simulate velocity vs field for various mobility values. Of particular interest in this simulation was ensuring proper velocity overshoot. Figures 3-1 and 3-2 show curves fit to the results of Monte Carlo simulations for various mobility values and for the mobility in GaN at various temperatures. This project will focus on operation at 300K, but higher and lower temperature behavior is a valuable topic for future research.

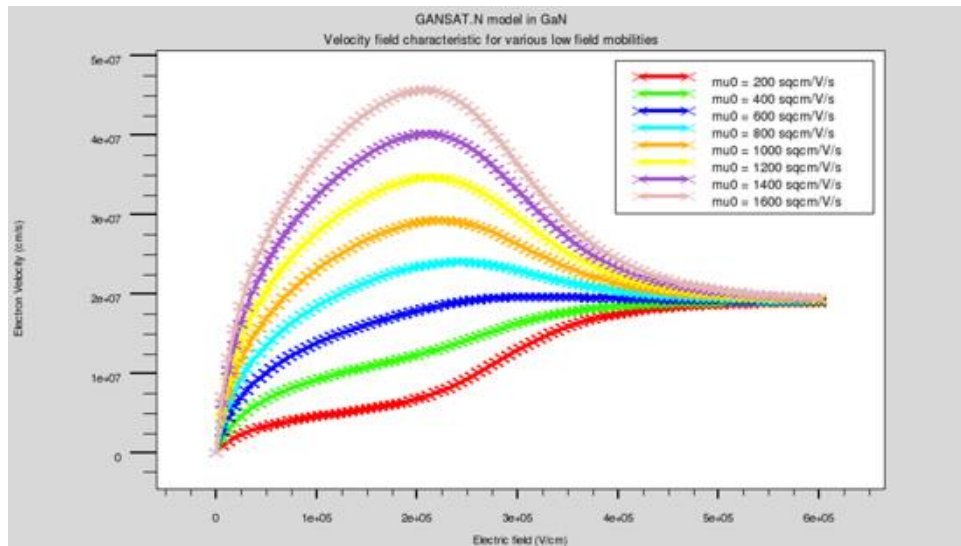


**Figure 3-1: Monte Carlo Simulation of GaN Electron Velocity vs Electric Field [1].**

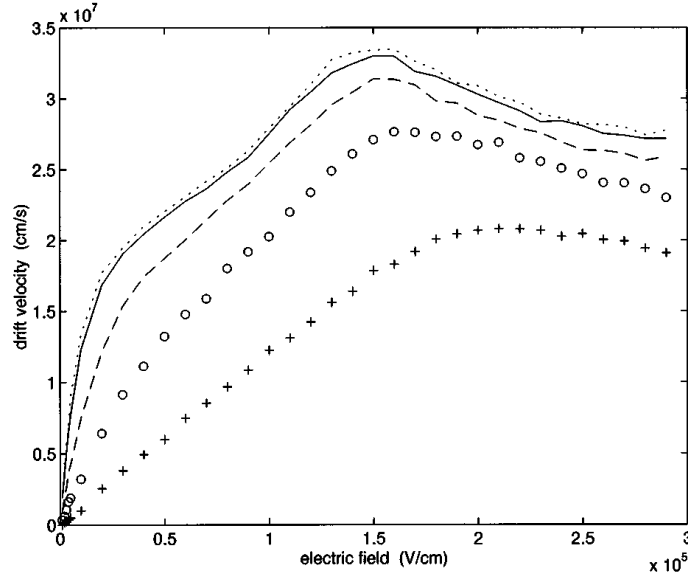


**Figure 3-2: GaN Electron Velocity vs Field for Nd=1E17 at 77K (Dotted), 150K (Solid), 300K (Dashed), 500K (Circles), and 1000K (Pluses) [4].**

Velocity overshoot is a key characteristic of GaN and other III-V compound semiconductors, thus it is important to use a model that will account for this behavior. Velocity overshoot occurs when carriers in the central valley with low effective mass gain a high enough energy to transition to one of the satellite valleys with higher effective mass [17]. Since the carriers in the central valley have a lower effective mass, they can reach a higher average velocity between scattering events than the carriers in the satellite valleys. This leads to the overshoot in the velocity vs field curve when the carriers have a high mobility. In Silvaco Atlas, the simulation of this behavior is handled by the GANSAT.N and GANSAT.P mobility models. This model uses a curve fit to Monte Carlo data for bulk material [14].

To test the velocity overshoot characteristics for GaN, a simple simulation was setup in Atlas with a 20x20  $\mu\text{m}$  region of intrinsic GaN with contacts at the top and bottom. The voltage across the sample was swept from 0 to 1200 V in order to create an electric

field from 0 to 6E5 V/cm. To collect results, “PROBE” statements for the electric field and carrier velocity were setup in the center of the sample and recorded in a log file.

In order to accurately model a device in Atlas, the appropriate methods, models, and application specific parameters must be specified. A blanket set of methods including “Gummel”, “Block”, and “Newton” were specified for performing the simulation. Each of these methods has its advantage in certain applications and when specified together, Atlas will try the first method, then move on the second and third if the previous method did not converge in the default or user specified number of iterations. The Gummel method is useful for finding solutions with a rough initial guess, but converges slowly. The Block method is useful for simulations that involve lattice heating or where energy balance equations are used. The Newton method is useful for fast convergence, but requires a good initial solution [14]. In addition to these methods, the “Trap” and “carriers=1 electrons” parameters were also specified. These indicate that the bias step should be reduced if the solution does not converge and that only electrons should be simulated.

The proper models for this simulation took some time to establish as many override user set mobility values or caused convergence issues for this simulation. Models to avoid when simulating with manually specified mobility include `cvt`, `hcte.el`, `conmob`, `analytic`, `albrect.n`, `ccsmob`, and `fldmob`. The models ultimately used for this simulation include “SRH”, “Fermi”, and “impact selb”. The Shockley-Read-Hall (SRH) model implements fixed minority carrier lifetimes and is typically used in all simulations, the Fermi model implements Fermi carrier statistics, and “impact selb” is an impact statement that enables the impact ionization model and is also recommended for most

simulations [2]. The “conSRH” and “auger” models were also tested and yielded identical results to the previous models. The “conSRH” model implements SRH recombination with concentration dependent lifetime while the “Auger” model implements Auger recombination, important for high carrier concentrations [2].

The only material specific parameters used for this simulation was the mobility. For the mobility statements, “GANSAT.N” was used as the mobility model, “vsatn” (saturation velocity) was set to  $2.5E7$  cm/sec, and “mun0” was stepped through each mobility value tested. Figure 3-3 shows the result of the simulation.

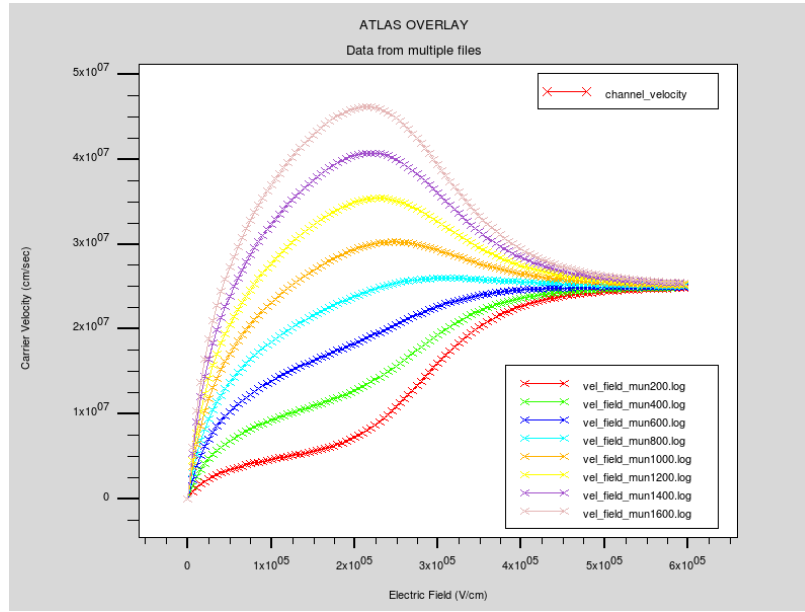


**Figure 3-3: Simulated Results for Mobility Values of 200 to 1600  $\text{cm}^2/\text{V}/\text{sec}$ .**

As expected, with the proper setup, the results exactly match the GANSAT.N model’s curves. In Figure 3-2, the 300 K curve has a peak velocity just above  $3E7$  cm/sec at about  $1.5E5$  V/cm. This peak velocity corresponds to approximately the level of the  $1000 \text{ cm}^2/\text{V}/\text{sec}$  curve, however the electric field at which it occurs is about  $1E5$  V/cm lower. This may be due to the sample having an n-type doping concentration of  $1E17$  or

that it is based on another Monte Carlo simulation who's input parameters may have varied from those used to fit the GANSAT.N curve. These differences open the possibility for further experimentation with different doping levels, temperatures, and comparisons to other models to assess the accuracy of the GANSAT model used in Atlas.

### 3.2 Device Simulation Setup

With the knowlage that the mobillity model was working and what methods and models should be used with it, the exparimental device described in Ch 2 was then recreated in Atlas. Since the experimental device was circular, the simulated device uses appoximatly equivelent rectangular dimmensions, meaning the width of the device was initially set to match the aperture perimiter of the circular device. The characteristics of a rectangular device however, are not exactly analigous to a dimensionally equivilent circular device, so some mismatch is expected. In particular, the corners in a rectangular device create high field regions not seen in circular devices Figure 3-5 shows a cross section of the simulated device structure.

After setting up the basic structure, it was important to refine the mesh such that it was fine enough in critical areas to produce quality results, but not so fine that it causes long simulation times and large log files. In a CAVET, the critical areas are near the contacts, under the gate, in the channel, and in the aperture. It also important to have a fine mesh anywhere a large current density or electric field is present. Figure 3-4 shows the fine mesh in the channel and aperture.

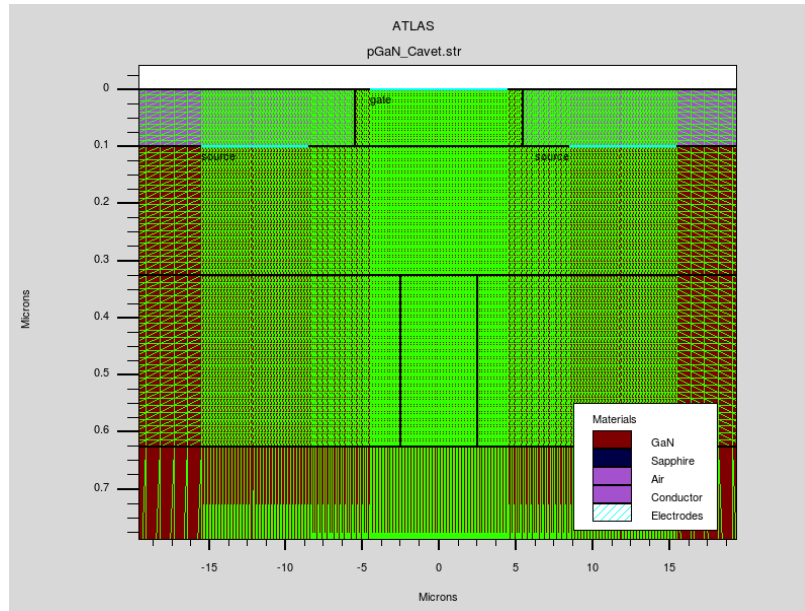


**Figure 3-4: Simulated Device Mesh Around the Channel and Aperture.**

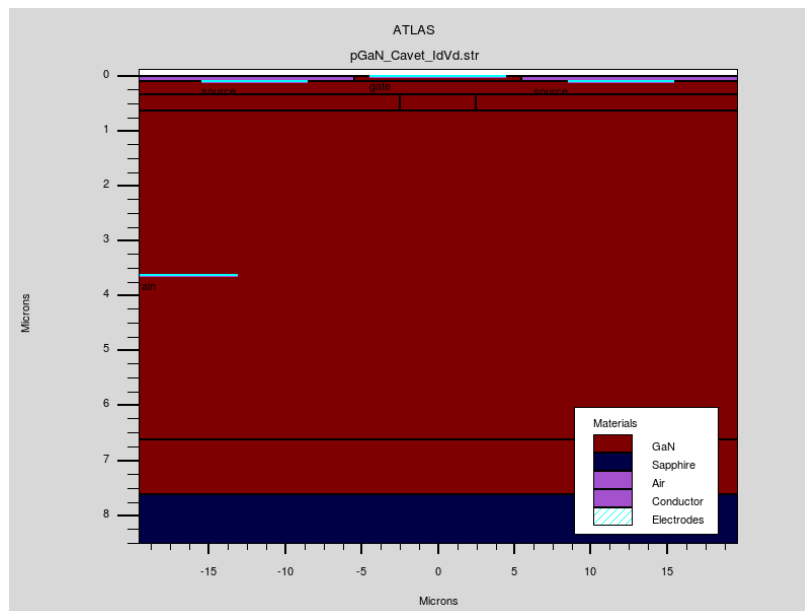


**Figure 3-5: Simulated Device Cross Section.**

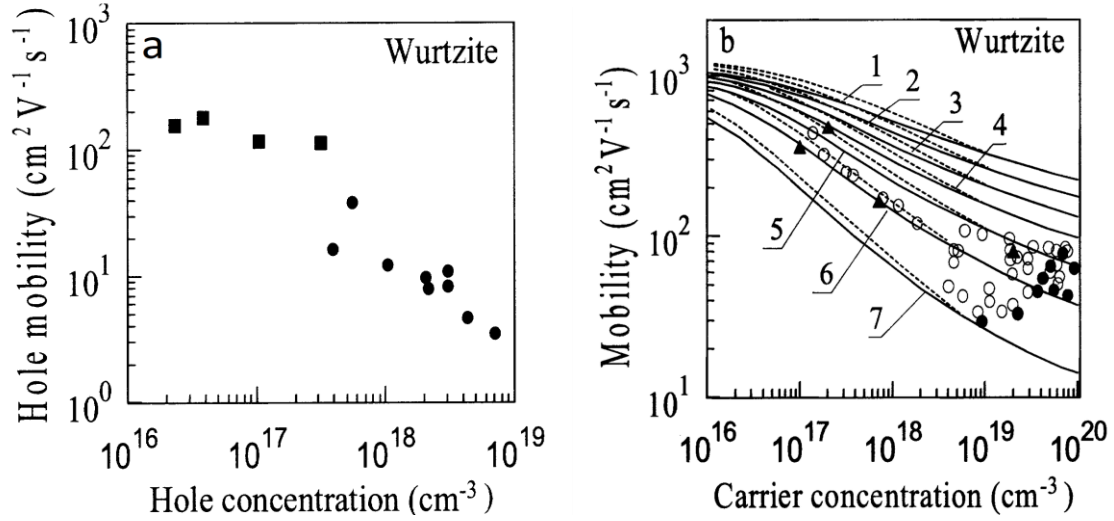


**Figure 3-6: (a) GaN Hole Mobility vs Concentration [13]. (b) GaN Electron Mobility vs Concentration for Various Compensation Values [6].**

As with the velocity overshoot simulation, the mobility for each region in the device was specified manually. The mobility values were approximated and assigned to each region based on doping concentration as shown in figure 3-6 (b). According to [12], auto compensation in n-type GaN for concentrations between  $1\text{E}17$  and  $1\text{E}20 \text{ cm}^{-3}$  results in a roughly constant compensation ratio ( $N_A/N_D$ ) of 0.7. This roughly corresponds to line 6 in figure 3-6 (b), representing 0.75. Table 3-1 shows the regions of the device with their respective doping and mobility.

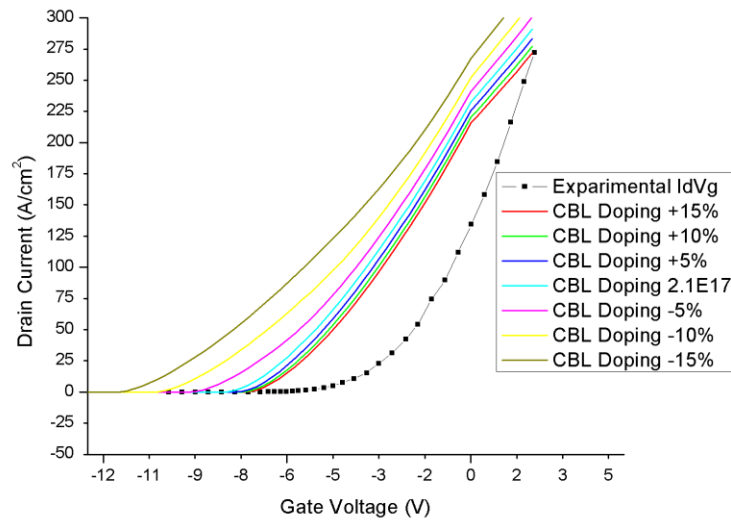
**Table 3-1: Mobility from Doping**

Region	Doping ( $\text{cm}^{-3}$ )	Mobility ( $\text{cm}^2/\text{V}/\text{sec}$ )
Channel	$3\text{E}17$	300
Aperture	$2\text{E}16$	800
Drift	$5\text{E}15$	1100
Drain	$2\text{E}18$	100



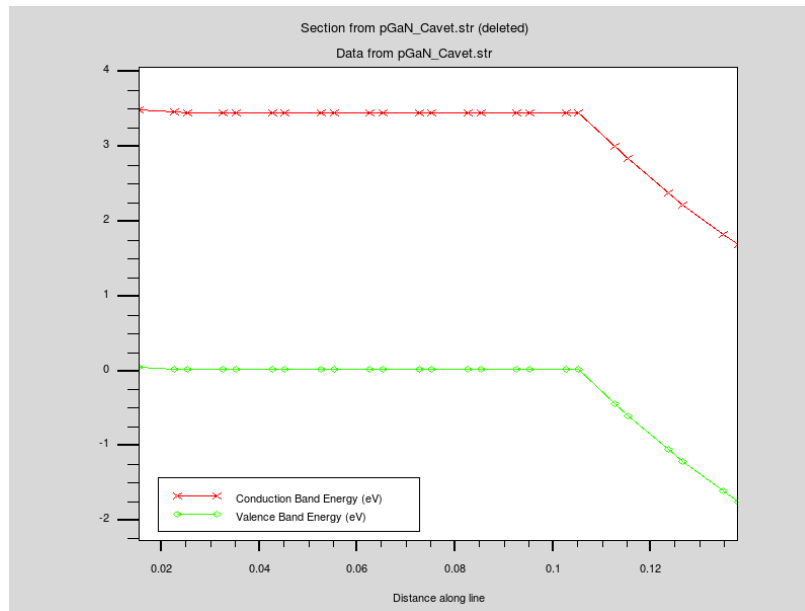
### 3.3 Parametric Sweeps

While refining the simulated device, the primary measure of how well the device was matched was its similarity to the ID-VG curve, and thus the transconductance, of the experimental device. With matched transconductance the device should perform identical to the experimental device for both the ID-VG and ID-VD curves. After completing the initial simulations, the current and slope (transconductance) of the ID-VG curve was not well matched to the experimental data. In order to narrow down the issue, a number of parameter sweeps were performed to show what parameter(s) would bring the simulation closer to the experimental data. These sweeps also have the benefit of illustrating the effects each parameter has on device performance as a whole and may be useful for understanding the characteristics of CAVETs and how to troubleshoot issues with other CAVETs or similar devices. Figure 3-7 shows an early sweep of the CBL doping with the curve getting closer to the appropriate transconductance with higher CBL doping.



**Figure 3-7: CBL Doping Sweep**

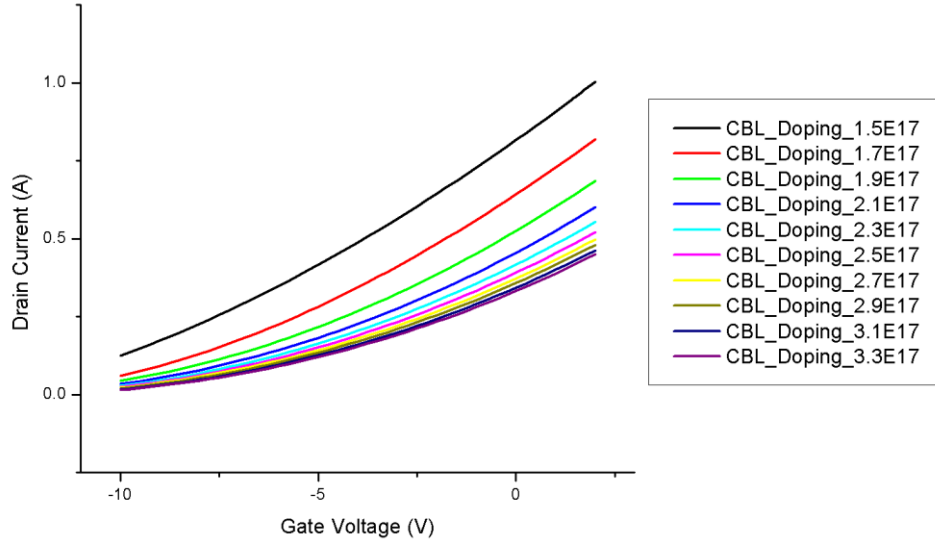
It should also be noted in Figure 3.7 that there is an inflection in the curves around the zero crossing. It was eventually determined that this seemed to be due to gate workfunction mismatch. The initial gate workfunction had been set to 5.2 eV, while a workfunction of 7.8 eV is what was required to achieve a flat conduction and valance band from the gate to the pGaN gate insulator. The conduction and valance bands from the gate, through the gate insulator, and into the channel are shown in Figure 3-8.



**Figure 3-8: Conduction and Valence Band Energy Through the Gate, pGaN Insulator and into the Channel.**

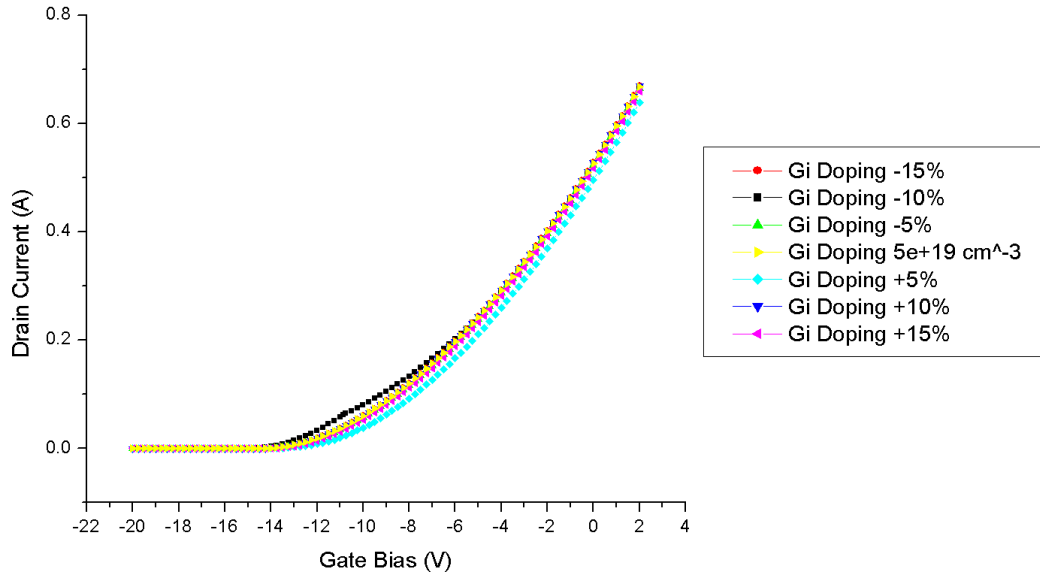
Figure 3-9 shows an extended CBL doping sweep from  $1.5\text{E}17$  to  $3.3\text{E}17 \text{ cm}^{-3}$  with the corrected gate workfunction. This extended sweep illustrates the diminishing returns that more extreme CBL doping increases will yield. CBL doping is therefore most effective for small transconductance changes to the ID-VG curve. The CBL doping was the primary focus of the initial sweeps since it was more loosely defined as an implant dose and intensity rather than a set value. With an accurate simulation being the goal,

every attempt was made to keep the simulated device as close to the physical device as possible.



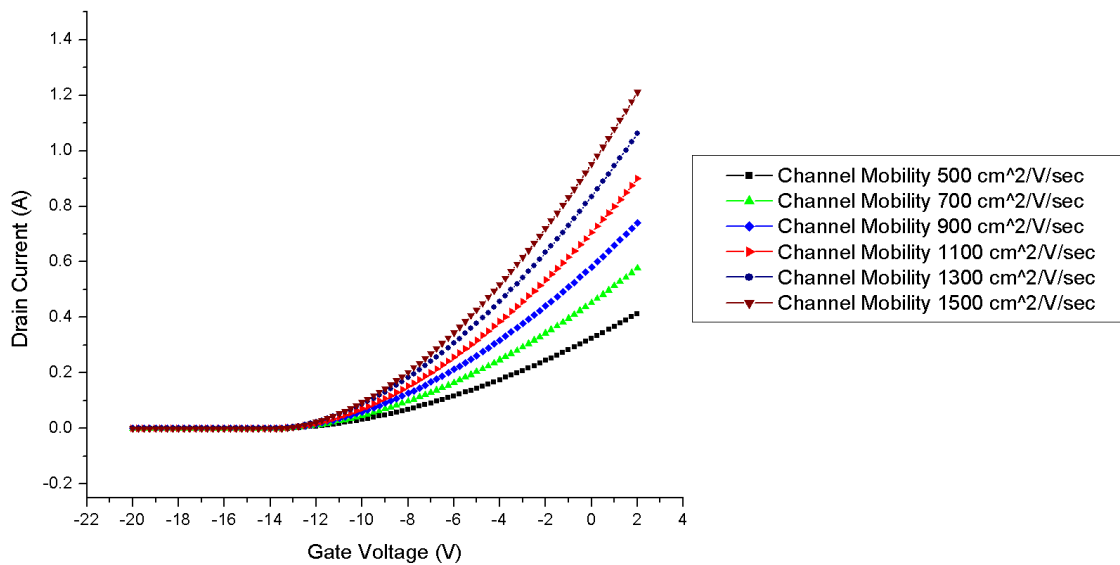
**Figure 3-9: Extended CBL Doping Sweep**

Figure 3-10 shows the effects of varying the gate insulator doping  $\pm 15\%$  in 5% increments from the value called for in the experimental device. For this small of a variation, some pinchoff shift can be seen, though ultimately the effect is negligible.



**Figure 3-10: Gate Insulator Doping Sweep**

The next sweep takes the mobility of the channel from 500 to 1500  $\text{cm}^2/\text{V}/\text{sec}$ . Figure 3-11 shows the transconductance and peak current of the ID-VG curve increasing with increasing mobility. This response makes intuitive sense, however there is not much margin for changing the mobility of the channel while still remaining true to a similarly doped physical device.



**Figure 3-11: Channel Mobility Sweep**

The remaining three mobility sweeps are of the aperture, drift region, and drain region. These are shown in figures 3-12, 3-13, and 3-14 respectively. These three regions are not as influential on device performance as the channel, as illustrated by the negligible affect these wide mobility sweeps have on the ID-VG curve.

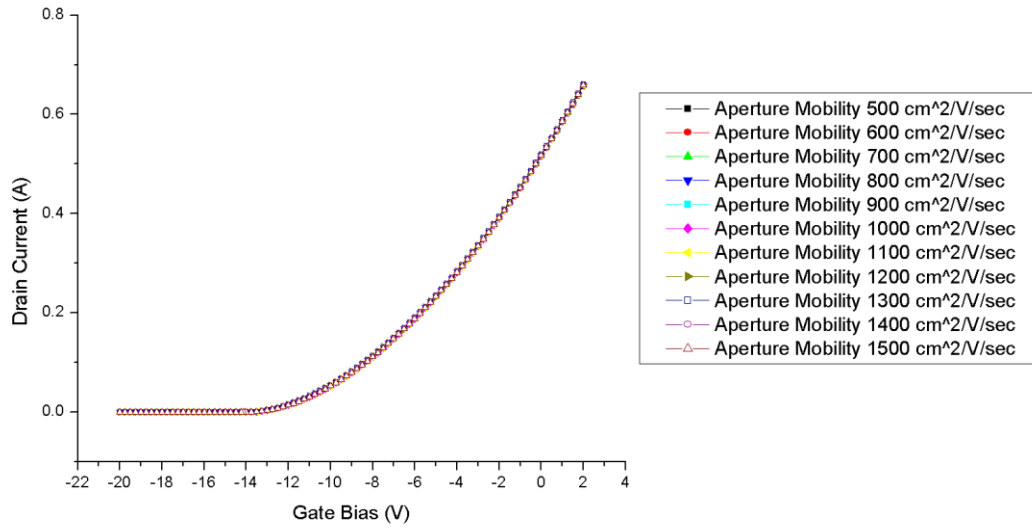


**Figure 3-12: Aperture Mobility Sweep**

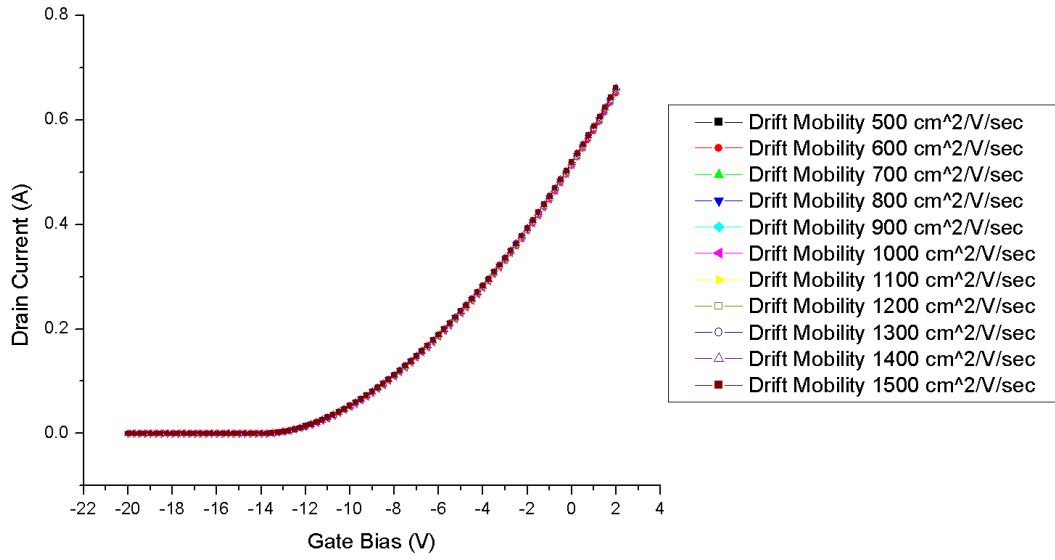


**Figure 3-13: Drift Region Mobility Sweep**

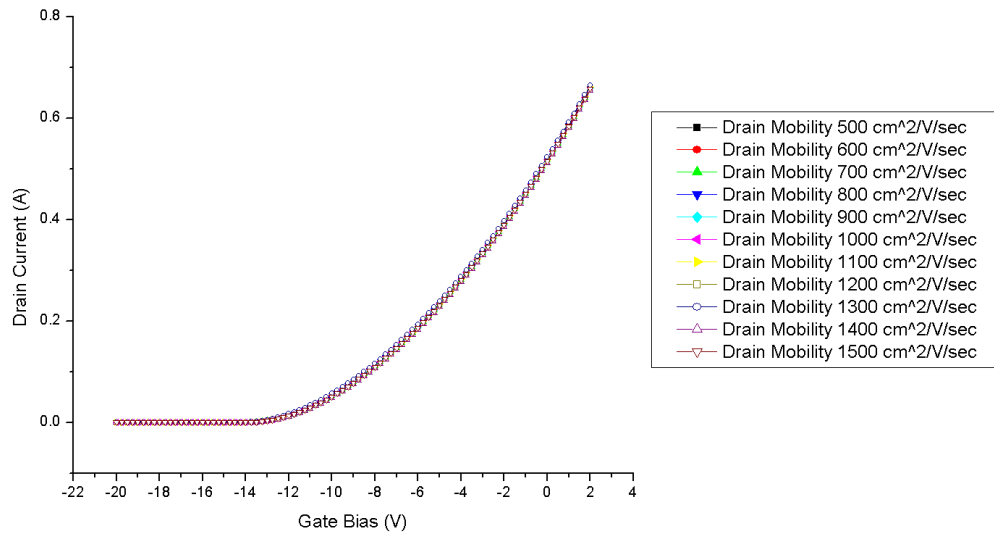


**Figure 3-14: Drain Region Mobility Sweep**

The gate overlap sweep from 1 to 7  $\mu\text{m}$  is shown in figure 3-15. This sweep appears to exhibit a similar behavior to the CBL doping change in that it changes the transconductance. This similarity may be due to both having the effect of further constraining the aperture, either through a stronger CBL or through the expansion of the depletion region below the gate that modulates the flow of carriers into the channel.

Unlike the CBL doping or gate overlap, the expansion of the aperture length itself has a negligible effect on the ID-VG curve, as shown in figure 3-16. This is a consequence of the simulated device's rectangular structure. Carriers travel along the walls of the aperture, therefore to have an appreciable effect on performance, changing the aperture length would have to expand the area of the wall carriers are traveling along. Since the carriers move vertically once they reach the aperture and the sources are only located to the left and right, the aperture wall area is controlled exclusively by the device width. This is the same way a traditional rectangular FET width works and modulates the transfer characteristic in the same way as well. Since the experimental device was circular, expanding the aperture would increase the area for carriers to travel much like changing the width of the simulated device. Bearing this in mind, it may be more accurate to compare expanding the width of the simulated device to increasing the diameter of the aperture on the experimental device.

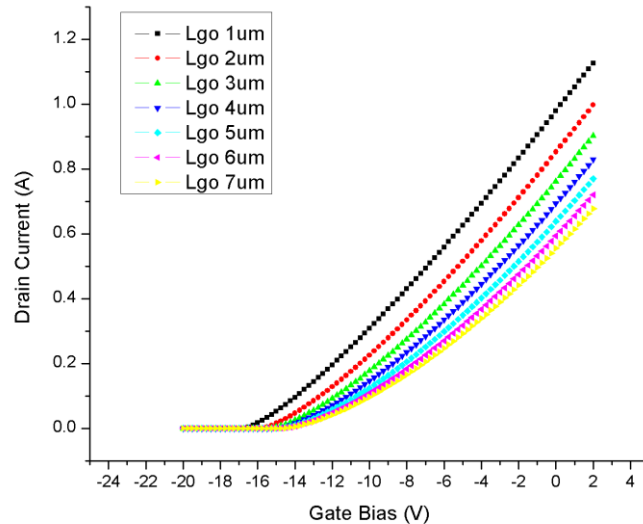


**Figure 3-15: Gate Overlap Sweep**

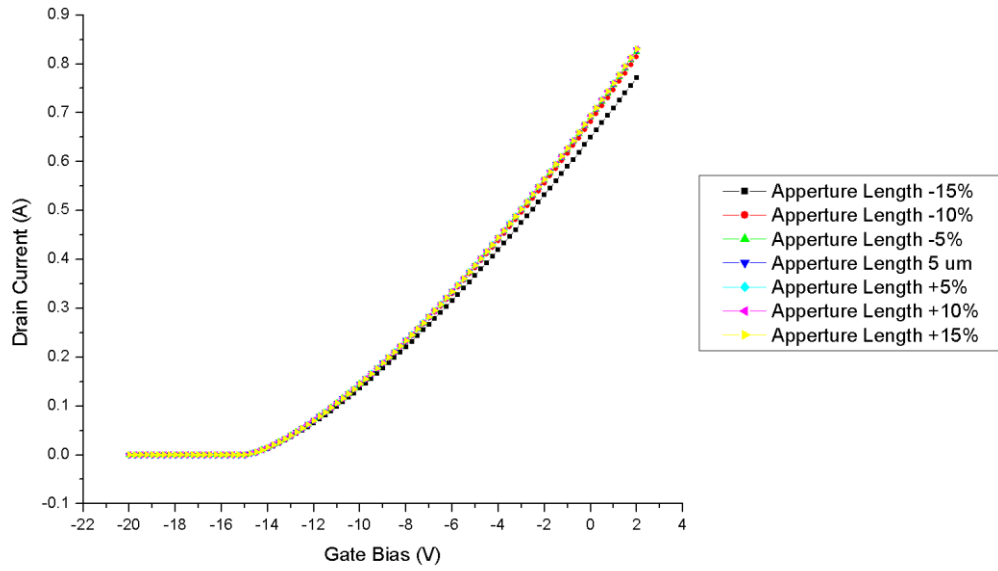


**Figure 3-16: Aperture Length Sweep**

Figure 3-17 shows a large sweep of the drain contact resistance. Like several of the drain, drift, and aperture mobility values, this has little effect on the ID-VG curve until it is taken to an extreme, as seen in the highest resistance. Though the drain and internal resistances have made little difference in the ID-VG curves in these simulations, they tend to become much more pronounced in the ID-VD curves.

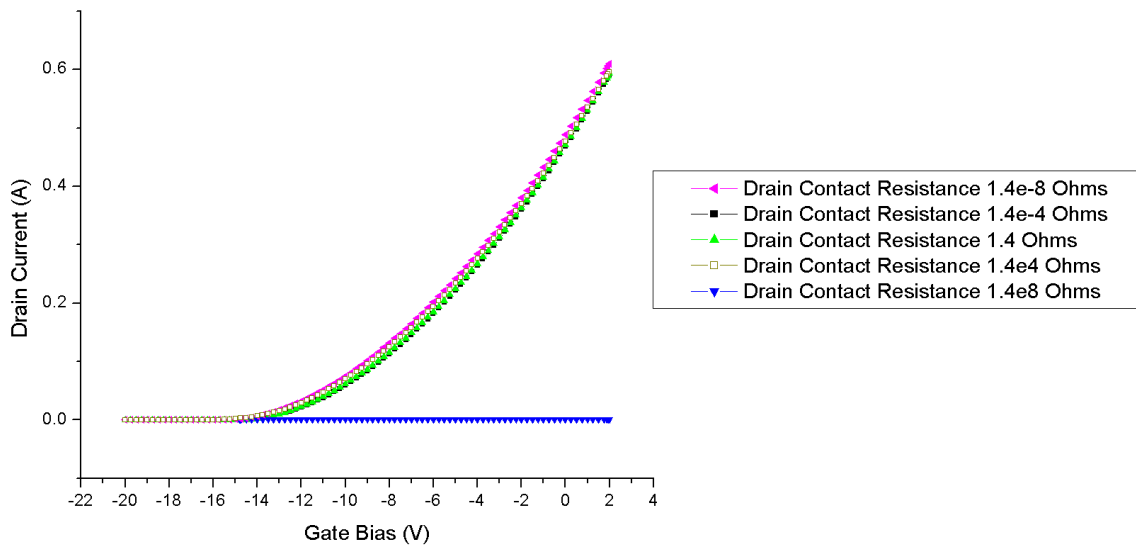


**Figure 3-17: Drain Resistance Sweep**



Finally, the last sweep is of the channel thickness. Shown in figure 3-18, adjusting the channel thickness results in a fairly linear scaling of the current and threshold without changing the transconductance. Since current (coulombs/sec) is a function of the number of carriers that pass through per unit time, for the same current density, thinning or expanding the channel (and thus the cross sectional area that carriers have to flow through it) could increase or decrease the current as shown. Additionally, since capacitance is in the denominator of the threshold equation, thinning the channel can lead to higher capacitance and reduced threshold, or in the case of a depletion mode device like the CAVET, a less negative threshold.

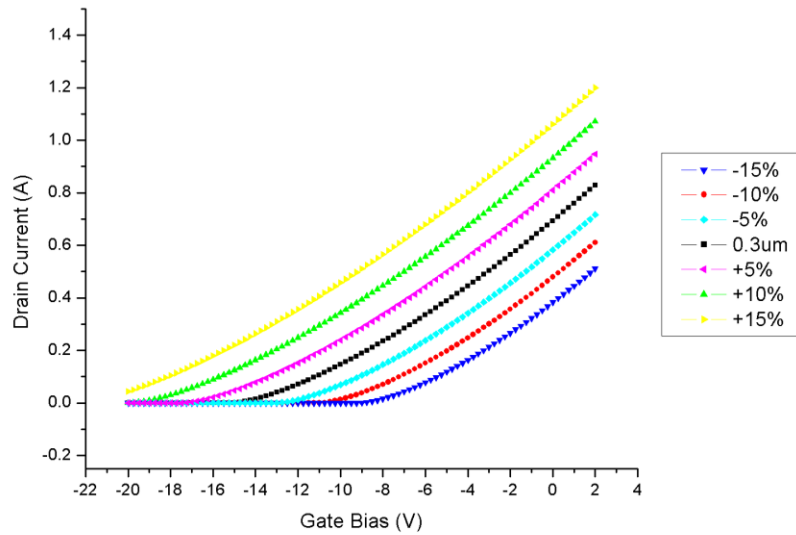


**Figure 3-18: Channel Thickness Sweep**

### 3.4 Final Setup and Results

From the parametric sweeps, it was determined that adjustment of the CBL doping, channel thickness, and device width provided the corrections necessary to bring the

simulated device into alignment with the experimental device. All else staying the same, the corrections are listed in table 3-2.

**Table 3-2: Corrected Values**

Feature	Corrected value
CBL Doping ( $\text{cm}^{-3}$ )	2.1E17
Channel Thickness ( $\mu\text{m}$ )	0.2255
Device Width (mm)	1.1

Both the CBL and device width seem to be reasonable for this device, however the amount it was necessary to change the channel thickness is somewhat concerning since it accounts for a percent change of 28.35% less than the original. This may or may not be accounted for in the geometric difference between the two CAVETs. With these changes, the final simulation result in an ID-VG curve (figure 3-19) that matches very well with the experimental data and ID-VD curves (figure 3-20) that are able to match the saturation current within a reasonable margin. Looking into the ID-VD curves, as noted in Ch 2, the shape of the experimental ID-VD curves would seem to imply that the device is very resistive. This resistance could come from the quality of the lattice and junctions within the device (such as the carbon doped layer) or perhaps with the contacts to the test equipment. The simulated device however, exhibits the expected quick rise to the saturation current. The results below have been converted to  $\text{A}/\text{cm}^2$  in order to match the presentation of the experimental results by dividing the drain current over the area between the source contacts.

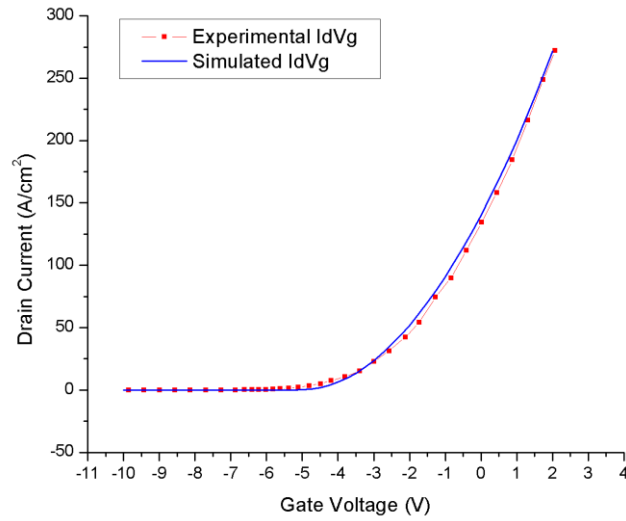


**Figure 3-19: Simulated ID-VG Curve and Experimental Data**

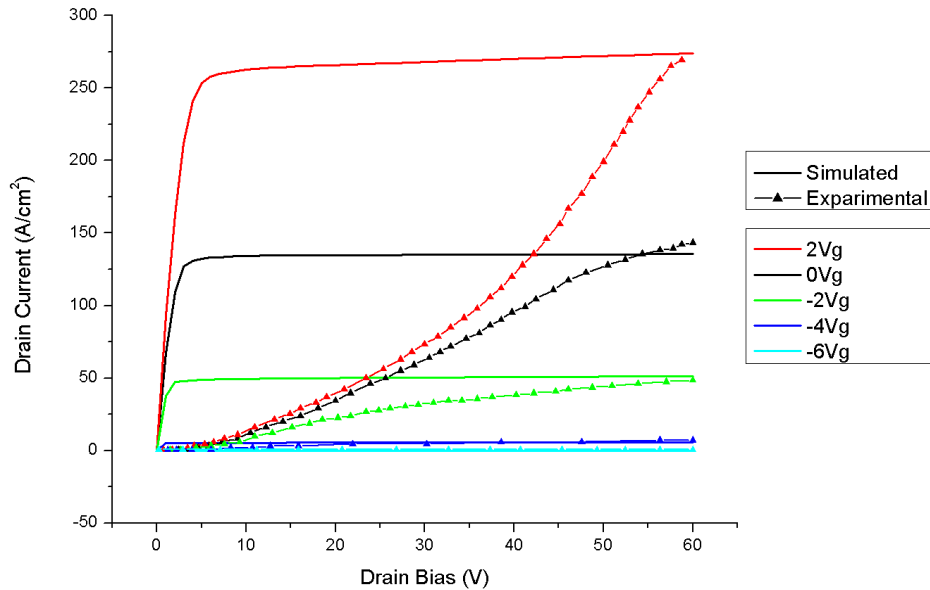


**Figure 3-20: Simulated and Experimental ID-VD Curves**

A breakdown simulation of the same device was performed by applying a gate bias of -10 V and sweeping the drain to 600 V. Atlas was set to run with 128 bit precision and drain bias steps of 0.25 V to improve breakdown accuracy and simulation convergence, though the simulation only made it to about 450 V before failing to converge. An extract statement was used to define the breakdown voltage as the point where current exceeded

1 mA. The result was a breakdown voltage of 278 V, considerably lower than the 422 V seen in the experimental device. The lower breakdown may be attributed the higher electric field at the edges of the rectangular aperture that are not present in a cylindrical device or the drain not being as far from the gate in the simulated device as it is in the experimental device. Also, it was noted in Ch 2 that the CBL was the limiting factor in the breakdown of the experimental pGaN insulated gate CAVET. Since the CBL doping was adjusted to obtain the desired ID-VG and ID-VD curves, this may have also played a role in reducing the breakdown voltage. Figure 3-21 show the breakdown curve.

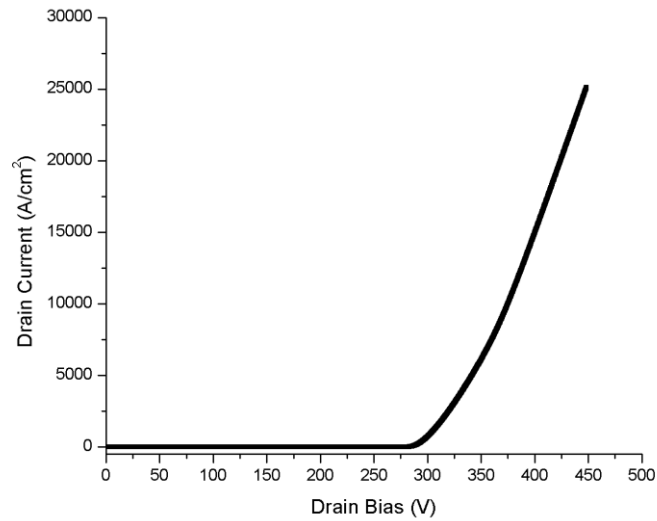


**Figure 3-21: Breakdown of the Simulated pGaN Insulated Gate CAVET**

Figures 3-22, 3-23, and 3-24 show the electron concentration, electric field magnitude, and impact ionization rate in the device at breakdown. The electron concentration shows the carriers are punching through the CBL rather than through the gate insulator, just as seen in the experimental device.

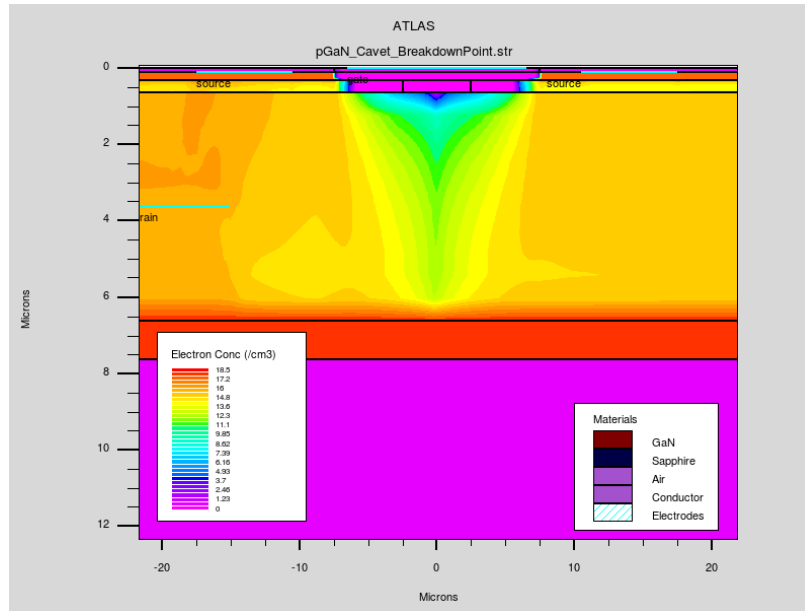


**Figure 3-22: Log Scale Electron Concentration at Breakdown ( $1 \times 10^x \text{ cm}^{-3}$ )**

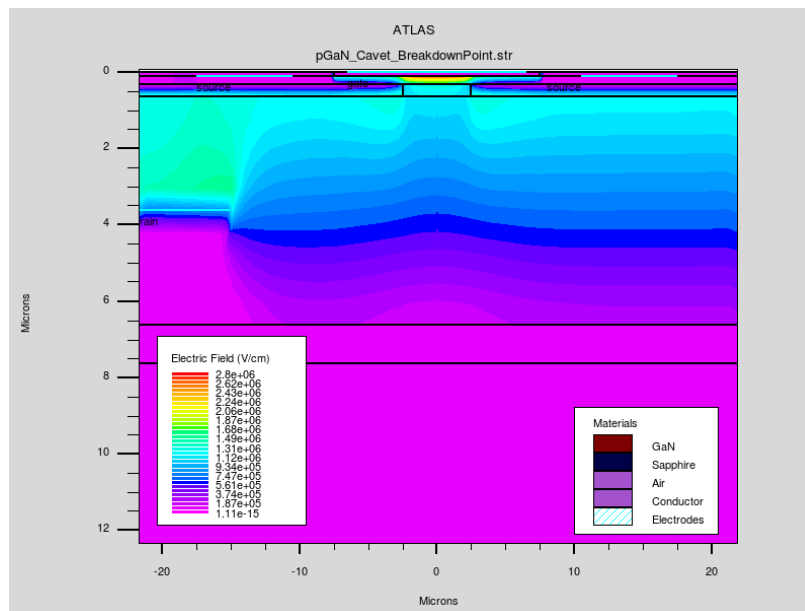


**Figure 3-23: Electric Field Magnitude at Breakdown**

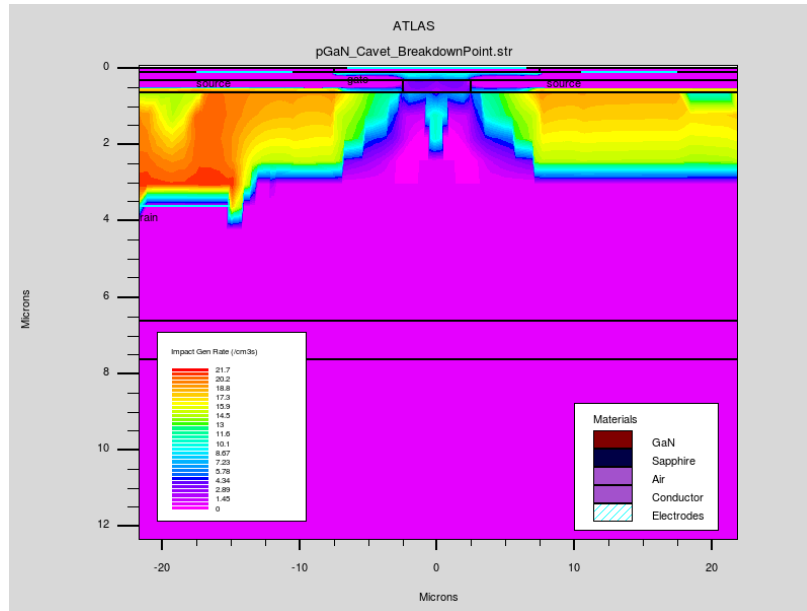


**Figure 3-24: Log Scale Impact Ionization Rate**

Figures 3-25 and 3-26 show the electron concentration and electric field within the device under the 70 V bias condition used in the ID-VG simulation and are included as a comparison to show how the CAVET normally operates.

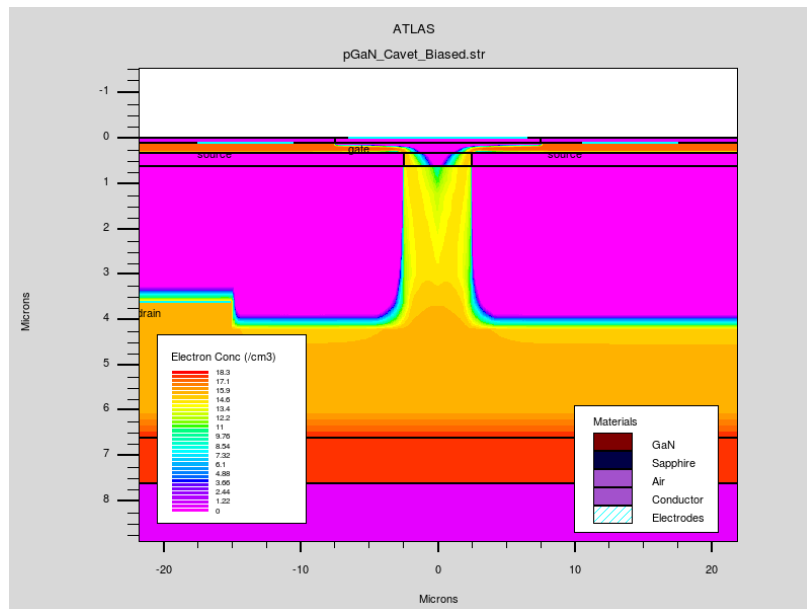


**Figure 3-25: Simulated Device Log Scale Electron Concentration at 70V Drain Bias.**

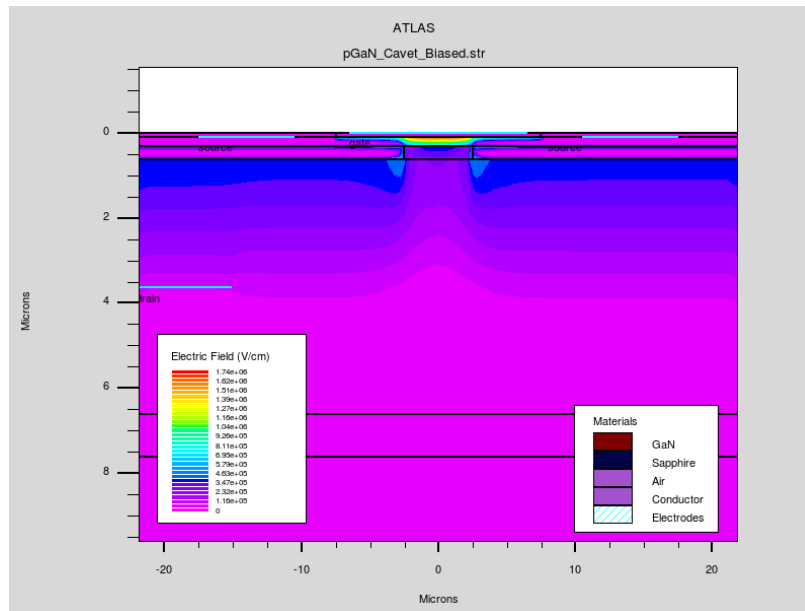


**Figure 3-26: Simulated Device Electric Field Profile at 70V Drain Bias.**

## Chapter 4

### Conclusion and Future Work



## 4.1 Conclusion

GaN based CAVETs have been shown to exhibit many desirable properties for high power high frequency operation, however relatively new and exotic materials and processing steps make them very expensive to experiment with physically. The solution is therefore to develop the proper techniques for GaN devices simulation in order to refine device designs before proceeding to physical prototypes.

The simulation of Mandal's pGaN insulated gate CAVET has shown that the following combination of simulation options works well for simulating ID-VG, ID-VD, and breakdown characteristics. For methods, it is recommended to use Gummel, Block, Newton, and Trap; for models, SRH, Fermi, Auger, and impact self; and finally for mobility, the use of the GANSAT model and manually specified saturation velocity and mobility based on doping concentration.

In addition to the proper simulation setup, several parametric sweeps were performed to highlight critical device parameters. These showed that, of those tested, critical parameters included channel mobility (and thus doping), channel thickness, CBL doping, gate overlap, and aperture width in rectangular devices or diameter in cylindrical devices.

It is the hope that the results covered in these simulation experiments will help to further the accurate simulation of GaN based devices, and in particular, that of CAVETs.

## 4.2 Future Work

Due to time constraints, it was necessary to forgo some of the simulations that were initially planned. Additionally, some of the results present opportunities for further

investigation. These are suggested as future work that may expand on this paper and advance the techniques for proper GaN CAVET simulation.

Perhaps the most interesting simulations that had to be cut in the interest of time were the simulation of device operation at various temperatures and self-heating. Mandal covers self-heating effects in section 3.7 of [8] by plotting pulsed I-V characteristics in which longer pulses result in smaller current at high drain bias. These effects are important for power devices to ensure the device will meet the design requirements when operating at temperature. This can be tested in Silvaco Atlas by including the “lat.temp” model for lattice heating and pulsing the gate and drain bias during an ID-VD output characteristic sweep.

This paper covered the simulation of Mandal’s single CBL implant pGaN insulated gate CAVET, however as mentioned in the experimental section, Mandal also tested a nearly identical box implant CAVET that had better output characteristics. Simulating this device could improve the results by perhaps showing better ID-VD curve matching beyond just the saturation current. In addition, it would be useful to simulate other CAVET devices such as those with an AlGaIn/GaN heterojunction in order to be more representative of the type of devices that may be used in real world applications. Silvaco Atlas is also capable of simulating cylindrical devices, so repeating the simulations described in this paper with a device more representative of the original would be a useful exercise.

Lastly, it was mentioned in the results that drain resistance had little effect on the ID-VG transfer characteristics, though it was suspected to have a much larger effect on the

ID-VD output characteristics. Therefore, another useful expansion on this work could be simulation of the ID-VD curves with a sweep of resistance in the drain and other locations throughout the device to characterize the effects.

## REFERENCES

- [1] Anonymous "State of the Art 2D and 3D Process and Device Simulation of GaN-Based Devices," *The Simulation Standard*, vol. 23, (3), pp. 1, Jul, 2013.
- [2] M. C. Allia, "Device Simulation,".
- [3] I. Ben-Yaacov *et al*, "AlGaIn/GaN current aperture vertical electron transistors with regrown channels," *J. Appl. Phys.*, vol. 95, (4), pp. 2073-2078, 02/15; 2019/03, 2004.
- [4] U. V. Bhapkar and M. S. Shur, "Monte Carlo calculation of velocity-field characteristics of wurtzite GaN," *J. Appl. Phys.*, vol. 82, (4), pp. 1649-1655, 1997.
- [5] S. Bloom *et al*, "Band Structure and Reflectivity of GaN," *Phys. Stat. Sol. (b)*, vol. 66, (1), pp. 161-168, 11/01; 2019/03, 1974.
- [6] V. W. L. Chin, T. L. Tansley and T. Osotchan, "Electron mobilities in gallium, indium, and aluminum nitrides," *J. Appl. Phys.*, vol. 75, (11), pp. 7365-7372, 06/01; 2019/03, 1994.
- [7] W. M. Haynes, *CRC Handbook of Chemistry and Physics, 92nd Edition*. Hoboken: CRC Press, 2011.
- [8] S. Mandal, "Gallium Nitride Vertical Devices for Power Electronics Applications," University of California Davis, 2017.
- [9] D. V. P. McLaughlin and J. M. Pearce, "Progress in Indium Gallium Nitride Materials for Solar Photovoltaic Energy Conversion," *Metallurgical and Materials Transactions A*, vol. 44, (4), pp. 1947-1954, 04/01, 2013.
- [10] T. Mimura, "The early history of the high electron mobility transistor (HEMT)," *IEEE Trans. Microwave Theory Tech.*, vol. 50, (3), pp. 780-782, 2002.
- [11] S. Nakamura and M. R. Krames, "History of Gallium-Nitride-Based Light-Emitting Diodes for Illumination," *Proc IEEE*, vol. 101, (10), pp. 2211-2220, 2013.
- [12] J. W. Orton and C. T. Foxon, "The electron mobility and compensation in n-type GaN," *Semiconductor Science and Technology*, vol. 13, (3), pp. 310-313, 03/01, 1998.
- [13] M. Rubin *et al*, "[ital p]-type gallium nitride by reactive ion-beam molecular beam epitaxy with ion implantation, diffusion, or coevaporation of Mg," *Appl. Phys. Lett.*, vol. 64, (1), 1994.
- [14] Silvaco, "Atlas User's Manual," 2016.

- [15] G. Stark, "Light," *Encyclopædia Britannica*, September 07, 2018, 2018.
- [16] M. Suzuki, T. Uenoyama and A. Yanase, "First-principles calculations of effective-mass parameters of AlN and GaN," *Phys.Rev.B*, vol. 52, (11), pp. 8132-8139, Sep, 1995.
- [17] S. L. Teitel and J. W. Wilkins, "Ballistic transport and velocity overshoot in semiconductors: Part I—Uniform field effects," *IEEE Transactions on Electron Devices*, vol. 30, (2), pp. 150-153, 1983.
- [18] R. J. Trew, M. W. Shin and V. Gatto, "High power applications for GaN-based devices," *Solid State Electronics*, vol. 41, (10), pp. 1561-1567, 1997.
- [19] W. Wessner, "Mesh Refinement Techniques for TCAD Tools.", Vienna University of Technology, 2006.

## APPENDIX A

### TRANSFER CHARACTERISTIC SIMULATION INPUT DECK

```

go internal
#####Lateral Dimensions#####
#Legth Aperture
set lap=5
#Length gate overlap
set lgo=4
#length gate
set lg=2*$lgo+$lap
#2*$lgo+$lap
#length gate to source
set lgs=4
#Length source
set ls=7
#length drain (same as source)
set ld=7
#Edge buffer
set edge=($lgo+$lap)/2

#####Vertical Dimensions#####
#thickness p-GaN gate insulator
set tgi=0.1
#thickness channel
set tch=0.2255
#0.226
#0.3
#Carbon doped GaN interlayer
set tcgan=0
#0.015
#Aperture/CBL thickness
set tcb1=0.3
#Drift layer
set tdrift=6
#base n+ GaN layer (Drain Region)
set tbase=1
#substraighnt thickness (tsubstrate>>teverythingelse)
set tsub=450

#Width of the device (in cm, not um)
set wdev=1.1e-1
#4.1e-1
#1.725e-1
#4e-1
#4.4e-1
#4.5e-1
#5.5e-1

#####Doping#####
#doping p-GaN gate insulator
set ngi=5e19
#doping channel
set nch=3e17
#Carbon doped GaN interlayer
set ncgan=1e14
#6e18
#CBL doping
set ncbl=2.1e17
#2.1e17
#1.5e17
#1.6e19
#Apperture doping
set nap=2e16
#Drift layer
set ndrift=5e15
#1e16
#base n+ GaN layer
set nbase=2E18
#3e18

#Mobility
#GaN mu n (cm^2/V*sec)

```

```

#channel mobility
set chanun=300
#800
#2000
#aperture
set apun=800
#1100
#drift region mobility
set driftun=1100
#base
set baseun=100
#600

#GaN saturation velocity
set ganvsat=2.5e7

#Polarization scale
set pol=0
#0.7

#Thermal Conductivity (W/cmK)
set tc_gan=1.3
#set tc_algan=2.86
set tc_sapph=0.33

#drain contact resistance
set drainres=($ld*1)*2e-11
#1.4e-6
#($ld*1)*2e-11
#($ld*9000)*2e-11

#go atlas

#start atlas with a bit precision of 128
#go atlas simflags="-128"

#start atlas with default bit precision (something like 64)
#-P simflag says how many processors to use in parallel. ASU computers have 12 usable
cores.
#go atlas simflags="-P 6"

go atlas

#####Mesh#####
set xm1div=5
set xm2div=35
set xm3div=25
set xm4div=20
set xm5div=50

mesh width=1000
#Left edge
x.m n=1 l=-(0.5*$lg+$lgs+$ls+$edge)
#left of left source
x.m n=1+$xm1div l=-(0.5*$lg+$lgs+$ls)
#under left source
x.m n=1+$xm1div+$xm2div l=-(0.5*$lg+$lgs)
#between left source and gate
x.m n=1+$xm1div+$xm2div+$xm3div l=(-0.5*$lg)
#between left gate edge and left aperture edge
x.m n=1+$xm1div+$xm2div+$xm3div+$xm4div l=-0.5*$lap
#center
x.m n=1+$xm1div+$xm2div+$xm3div+$xm4div+$xm5div l=0.5*$lap

x.m n=1+$xm1div+$xm2div+$xm3div+2*$xm4div+$xm5div l=0.5*$lg
x.m n=1+$xm1div+$xm2div+2*$xm3div+2*$xm4div+$xm5div l=0.5*$lg+$lgs
x.m n=1+$xm1div+2*$xm2div+2*$xm3div+2*$xm4div+$xm5div l=0.5*$lg+$lgs+$ls
x.m n=1+2*$xm1div+2*$xm2div+2*$xm3div+2*$xm4div+$xm5div l=0.5*$lg+$lgs+$ls+$edge

set ym1div=10

```



```

set ym2div=20
set ym3div=5
set ym4div=20
set ym5div=10
set ym6div=5
set ym7div=10

#top
y.m n=1 l=0
#in the gate insulator
y.m n=1+$ym1div l=$tgi
#in the channel
y.m n=1+$ym1div+$ym2div l=$tgi+$tch
#in the carbon doped GaN Interlayer
y.m n=1+$ym1div+$ym2div+$ym3div l=$tgi+$tch+$tcgan
#in the CBL and Aperture
y.m n=1+$ym1div+$ym2div+$ym3div+$ym4div l=$tgi+$tch+$tcgan+$tcbl
#in the drift/drain region
y.m n=1+$ym1div+$ym2div+$ym3div+$ym4div+$ym5div l=$tgi+$tch+$tcgan+$tcbl+$tdrift
#in the base layer
y.m n=1+$ym1div+$ym2div+$ym3div+$ym4div+$ym5div+$ym6div
l=$tgi+$tch+$tcgan+$tcbl+$tdrift+$tbase
#in the substreight
y.m n=1+$ym1div+$ym2div+$ym3div+$ym4div+$ym5div+$ym6div+$ym7div
l=$tgi+$tch+$tcgan+$tcbl+$tdrift+$tbase+$tsub

#####Regions#####

#gate insulator
#region num=1 material=GaN x.min=- (0.5*$lg+$lgs+$ls+$edge) x.max=0.5*$lg+$lgs+$ls+$edge
y.min=0 y.max=$tgi polarization calc.strain polar.scale=$pol
#region num=1 material=GaN x.min=- (0.5*$lg+$lgo+1) x.max=0.5*$lg+$lgo+1 y.min=0
y.max=$tgi polarization calc.strain polar.scale=$pol
region num=1 material=GaN x.min=- (0.5*$lg+1) x.max=0.5*$lg+1 y.min=0 y.max=$tgi
polarization calc.strain polar.scale=$pol
#channel Layer
region num=2 material=GaN x.min=- (0.5*$lg+$lgs+$ls+$edge) x.max=0.5*$lg+$lgs+$ls+$edge
y.min=$tgi y.max=$tgi+$tch polarization calc.strain polar.scale=$pol
#Carbon doped GaN layer
region num=3 material=GaN x.min=- (0.5*$lg+$lgs+$ls+$edge) x.max=0.5*$lg+$lgs+$ls+$edge
y.min=$tgi+$tch y.max=$tgi+$tch+$tcgan polarization calc.strain polar.scale=$pol
#Left CBL Layer
region num=4 material=GaN x.min=- (0.5*$lg+$lgs+$ls+$edge) x.max=0- (0.5*$lap)
y.min=$tgi+$tch+$tcgan y.max=$tgi+$tch+$tcgan+$tcbl polarization calc.strain
polar.scale=$pol
#Aperture
region num=5 material=GaN x.min=0- (0.5*$lap) x.max=(0.5*$lap) y.min=$tgi+$tch+$tcgan
y.max=$tgi+$tch+$tcgan+$tcbl polarization calc.strain polar.scale=$pol
#Right CBL Layer
region num=6 material=GaN x.min=(0.5*$lap) x.max=(0.5*$lg+$lgs+$ls+$edge)
y.min=$tgi+$tch+$tcgan y.max=$tgi+$tch+$tcgan+$tcbl polarization calc.strain
polar.scale=$pol
#Drift Layer
region num=7 material=GaN x.min=- (0.5*$lg+$lgs+$ls+$edge) x.max=0.5*$lg+$lgs+$ls+$edge
y.min=$tgi+$tch+$tcgan+$tcbl y.max=$tgi+$tch+$tcgan+$tcbl+$tdrift polarization
calc.strain polar.scale=$pol
#Base Layer
region num=8 material=GaN x.min=- (0.5*$lg+$lgs+$ls+$edge) x.max=0.5*$lg+$lgs+$ls+$edge
y.min=$tgi+$tch+$tcgan+$tcbl+$tdrift y.max=$tgi+$tch+$tcgan+$tcbl+$tdrift+$tbase
polarization calc.strain polar.scale=$pol
#Substrate
region num=9 material=Sapphire x.min=- (0.5*$lg+$lgs+$ls+$edge)
x.max=0.5*$lg+$lgs+$ls+$edge y.min=$tgi+$tch+$tcgan+$tcbl+$tdrift+$tbase
y.max=$tgi+$tch+$tcgan+$tcbl+$tdrift+$tbase+$tsub substrate name=substrate

region num=10 material=air x.min=- (0.5*$lg+$lgs+$ls+$edge) x.max=- (0.5*$lg+1) y.min=0
y.max=$tgi
region num=11 material=air x.min=(0.5*$lg+1) x.max=0.5*$lg+$lgs+$ls+$edge y.min=0
y.max=$tgi

#####Electrodes#####

```

```

#left source
electrode num=1 name=source x.min=-(0.5*$lg+$lgs+$ls) x.max=-(0.5*$lg+$lgs) y.min=$tgi
y.max=$tgi
#right source
electrode num=2 name=source x.min=(0.5*$lg+$lgs) x.max=(0.5*$lg+$lgs+$ls) y.min=$tgi
y.max=$tgi
#gate
electrode num=3 name=gate x.min=(-0.5*$lg) x.max=(0.5*$lg) y.min=0 y.max=0
#drain
#electrode num=4 name=drain x.min=-0.5*$lg+$lgs+$ls+$edge x.max=-0.5*$lg+$lgs+$ls+$edge
y.min=$tgi+$tch+$tcgan+$tcbl+0.5*$tdrift-0.25*$tdrift
y.max=$tgi+$tch+$tcgan+$tcbl+0.5*$tdrift+0.25*$tdrift

#electrode num=4 name=drain x.min=(-0.5*$lg) x.max=(0.5*$lg)
y.min=$tgi+$tch+$tcgan+$tcbl+$tdrift+$tbase y.max=$tgi+$tch+$tcgan+$tcbl+$tdrift+$tbase
electrode num=4 name=drain x.min=-(0.5*$lg+$lgs+$ls+$edge) x.max=-
(0.5*$lg+$lgs+$ls+$edge)+$ld y.min=$tgi+$tch+$tcgan+$tcbl+0.5*$tdrift
y.max=$tgi+$tch+$tcgan+$tcbl+0.5*$tdrift

#####Doping#####
doping region=1 uniform conc=$ngi p.type
doping region=2 uniform conc=$nch n.type
#doping region=3 uniform conc=$ncgan carbon
#doping trap region=3 e.level=2.85 uniform conc=$ncgan/4
#doping trap region=3 e.level=1.8 uniform conc=$ncgan/4
#doping trap region=3 e.level=0.5 uniform conc=$ncgan/4
#doping trap region=3 e.level=3.28 uniform conc=$ncgan/4

#doping trap region=3 acceptor sigp=5e-12 sign=5e-12 e.level=1.24 uniform conc=$ncgan/4
#doping trap region=3 donor sign=1.5e-11 sigp=1.5e-11 e.level=0.99 uniform conc=$ncgan/4
#doping trap region=3 donor sign=9.6e-16 sigp=9.6e-16 e.level=0.252 uniform conc=$ncgan

doping region=4 uniform conc=$ncbl p.type
#doping region=4 gaussian conc=$ncbl p.type characteristic=0.0625 x.left=-
(0.5*$lg+$lgs+$ls+$edge) x.right=0-(0.5*$lap) peak=$tgi+$tch+$tcgan+0.075
doping region=5 uniform conc=$snap n.type
doping region=6 uniform conc=$ncbl p.type
#doping region=6 gaussian conc=$ncbl p.type characteristic=0.0625
x.right=(0.5*$lg+$lgs+$ls+$edge) x.left=(0.5*$lap) peak=$tgi+$tch+$tcgan+0.075
doping region=7 uniform conc=$ndrift n.type
doping region=8 uniform conc=$nbase n.type

#####
# KM parameter set
#####
#material material=GaN eg300=3.4 align=0.8 permitt=9.5 \
mun=900 mup=10 vsatn=2e7 nc300=1.07e18 nv300=1.16e19 \
real.index=2.67 imag.index=0.001 \
taun0=$lt taup0=$lt

#####Contacts#####
#drain resistance=2e-11 ohms/um^2 * drain area (Default Silvaco device width is 1um)
contact name=drain resistance=$drainres

#set gate workfunction (Pd work function=5.2-5.6eV)
contact name=gate workfun=7.8
#5.2

#####mobility#####
#channel
#mobility region=2 gansat.n mun0=$chanun vsatn=$ganvsat betan=1.3 FMCT.N
mobility region=2 gansat.n gansat.p mun0=$chanun mup0=8 vsatn=$ganvsat betan=1.3
#FMCT.N FMCT.P
#aperture
#mobility region=5 gansat.n mun0=$apun vsatn=$ganvsat betan=1.3 FMCT.N
mobility region=5 gansat.n gansat.p mun0=$apun mup0=8 vsatn=$ganvsat betan=1.3
#FMCT.N FMCT.P
#drift region
#mobility region=7 gansat.n mun0=$driftun vsatn=$ganvsat betan=1.3 FMCT.N
mobility region=7 gansat.n gansat.p mun0=$driftun mup0=8 vsatn=$ganvsat betan=1.3
#FMCT.N FMCT.P

```

```

#base
#mobility region=8 gansat.n mun0=$baseun vsatn=$ganvsat betan=1.3 FMCT.N
mobility region=8 gansat.n gansat.p mun0=$baseun mup0=8 vsatn=$ganvsat betan=1.3
#FMCT.N FMCT.P

#####Models#####
#fldmob for 300k only
model SRH Fermi auger
#fldmob auger Fermi
#thermal fldmob lat.temp Fermi fldmob

#####Thermal Contacts#####
#thermcontact num=1 elec.num=1 ext.temp=300
#thermcontact num=2 elec.num=2 ext.temp=300
#thermcontact num=3 elec.num=3 ext.temp=300
#thermcontact num=4 elec.num=4 ext.temp=300
#thermcontact num=5 name=substrate ext.temp=300

#material material=GaN tc.cons=$tc_gan
#material material=sapphire tc.cons=$tc_sapph

output con.band val.band e.mobility h.mobility

#####Method#####
#method gummel block newton trap climit=1e-4 carriers=1 electrons
method gummel block newton trap carriers=2
#climit=1e-4
impact selb
#impact material=GaN selb an1=2.9e8 an2=2.9e8 bn1=3.4e7 bn2=3.4e7 \
ap1=2.9e8 ap2=2.9e8 bp1=3.4e7 bp2=3.4e7 e.side

#solve initial state, save, and display
solve init

save outfile=pGaN_Cavet.str
#tonyplot pGaN_Cavet.str

#####
#Solve
#####

set vstep=0.25
#set vstep=1
#vgate=-1
solve vdrain=0 vstep=$vstep*4 vfinal=70 name=drain
save outfile=pGaN_Cavet_Biased.str
#tonyplot pGaN_Cavet_Biased.str

log outfile=pGaN_Cavet_ID-VG.log
solve vgate=2 vstep=-$vstep vfinal=-10 name=gate
#extract name="Vth" (xintercept(maxslope(curve(abs(v."gate"),abs(i."drain"))))-
abs(ave(v."drain"))/2.0)
#extract name="Vth" (xintercept(maxslope(curve((v."gate"),(i."drain"))))-
(ave(v."drain"))/2.0)
#extract name="Pinchoff" x.val from curve(abs(v."gate"),abs(i."drain")) where y.val=0
#extract gm
#extract name="gm" abs(slope(minslope(curve(v."gate", i."drain"))))

## Transconductance (dId/dVg):
extract init infile="pGaN_Cavet_ID-VG.log"
extract name="gm" deriv(v."gate", i."drain"/10) \
outfile="pGaN_Cavet_ID-VG_gm.dat"
log off

#use the extract just to get the data into the same format so they overlay properly
#extract init infile="SaptarshiData.log"
#extract name="copy" curve(v."gate", i."drain") \
outfile="SaptarshiData.dat"
#log off

#extract init infile="SaptarshiData.log"

```

```

#extract name="gm" deriv(v."gate", i."drain"/10) \
outfile="SaptarshiData_gm.dat"
#log off

#Account for device width
extract init infile="pGaN_Cavet_ID-VG.log"
extract name="WidthMod" curve(v."gate", i."drain"/(($lap*1e-4+2*$lgo*1e-4+2*$lgs*1e-
4)*$wdev)) \
outfile="pGaN_Cavet_ID-VG_WidthMod.dat"
log off

#tonyplot -overlay pGaN_Cavet_ID-VG_WidthMod.dat SaptarshiData.dat
#tonyplot -overlay pGaN_Cavet_ID-VG_gm.dat SaptarshiData_gm.dat
tonyplot pGaN_Cavet_ID-VG_WidthMod.dat

quit

```